A descending interneuron with depolarized resting membrane potential controls *C. elegans* motor states

Jun Meng[1,2], Tosif Ahamed[2a], Bin Yu[3a], Wesley Hung[2], Sonia El Mouridi[4], Alice Leclercq-Blondel[4], Marie Gendrel[4,6], Zezhen Wang[5], Lili Chen[3], Quan Wen[5], Thomas Boulin[4], Shangbang Gao[3*], and Mei Zhen[1,2*]

[1]Department of Physiology, University of Toronto, Toronto, ON, Canada, [2]Lunenfeld-Tanenbaum Research Institute, Mount Sinai Hospital, Toronto, ON, Canada, [3]Huazhong University of Science and Technology, Wuhan, China, [4] Univ Lyon, Université Claude Bernard Lyon 1, MeLiS, CNRS UMR 5284, INSERM U1314, Institut NeuroMyoGène, Lyon 69008, France, [5]School of Life Sciences, University of Science and Technology, Hefei, Anhui, China, [6]Institut de Biologie de l'Ecole Normale Supérieure (IBENS), Ecole Normale Supérieure, CNRS, INSERM, Université Paris Sciences et Lettres Research University, Paris 75005, France

Mutually exclusive behaviors in animals are often driven by independent motor subcircuits that directly or indirectly inhibit each other. For example, in the nematode *C. elegans*, motor circuits for forward and backward locomotion are gated by premotor interneurons AVB and AVA respectively, which are thought to be connected via reciprocal inhibition. In this study, we dissect the interactions between forward and motor subcircuits in *C. elegans* by genetic manipulation of AVA's activity via cell-specific characterization of a two-pore potassium channel (TWK-40). AVA has an unusually depolarized resting membrane potential (RMP). Perturbations to its RMP through AVA-specific TWK-40 loss-of-function and AVA-specific TWK-40 gain-of-function, led to dramatic changes in both forward and backward motor activity. AVA, thus regulated both backward and forward locomotion in *C. elegans*, functioning as a master neuron for overall locomotion. These effects required chemical transmission from AVA and were dependent on AVB neurons. We were able to reconcile results of genetic perturbation with optogenetic manipulation by carefully designed stimulation protocols. Finding that phasic optogenetic activation of AVA leads to backward locomotion, while tonic optogenetic activation potentiates forward locomotion. These results propose that a single neuron can regulate the activity of motor circuits generating two mutually exclusive behaviors.

Introduction

The *C. elegans* motor system flexibly transitions between forward and backward locomotor states[1–4]. Two subcircuits of excitatory motor neurons (the B or A class) execute the forward and backward movement of the animal's body, respectively. Anatomically, two different classes of premotor interneurons (AVA and AVB) make electrical and chemical synapses with motor neurons of each subcircuit[5]. The activity of premotor interneurons AVA is correlated with and regulates reversals, whereas premotor interneurons AVB is associated with and drive forward locomotion. They were proposed to function as antagonizing models, resembling a flip-flop model[6].

The AVA have unique characteristics. Anatomically, it is not only the most heavily innervated descending interneuron, but the only premotor interneurons that are post-synaptic to all other premotor interneurons[5] across development[7]. Electrophysiologically, it also holds an unusually depolarized RMP, with several whole-cell patch-clamp recordings reporting RMP values around -20mV[8,9], likely maintained by two-pore potassium(K2P) and sodium leak channels. Functionally, AVA exerts a state-dependent dual modulation – inhibition and activation - of the A motor neurons' oscillatory activity for the backward motor circuit[2,3].

In this study, we examined the physiological requirement of AVA's excitability in intact *C. elegans* animals. First, we discovered and demonstrated that TWK-40, a K2P channel conducts an endogenous outward current in AVA. Through AVA-specific bidirectional changes of TWK-40's activity, we increased and decreased AVA's RMP, and examined the effect of altered intrinsic excitability of AVA in the motor circuit. We then compared and reconciled effects of changing AVA's membrane potential by genetic and optogenetic (Chrimson and GtACR2) manipulation leading to a functional model where phasic and tonic activation of AVA regulates both forward and backward locomotion in *C. elegans*.

This study demonstrates that investigating the property of membrane potential at single-neuron resolution is necessary to offer physiological insights into the underlying of the dynamic output of a neural circuit.

Results

A genetic toolkit to study motor behaviors in *C. elegans*

C. elegans has an expanded repertoire of K2P encoding genes. Each K2P gene is expressed in different subgroup of neurons[10], making them a potential genetic tool to dissect different neural circuits. To investigate how K2P-dependent neuronal activity regulates locomotory output, we targeted a putative K2P gene, *twk-40*, which is expected to regulate cellular excitability. We generated a loss-of-function allele, likely null, which harbors a 7 base pair deletion that leads to a frame-shift and truncation before the channel's first pore-forming domain, shared by all isoforms. This genetic lesion leads to a change in the animal's motor pattern with distinctive characteristics.

Wildtype animals use bending waves traveling along the body in opposite directions to perform forward and backward locomotion (Fig. 1C), showing a strong preference to the forward motor state [2]. However, compared to the wildtype animals, *twk-40(lf)* mutants exhibit more frequent transitions into the backward state and prolonged reversals, as well as increased curvature during both forward and backward movement (Fig. 1C, D). These changes indicate that a functional loss of TWK-40 increases overall motor activity of both forward and backward states.

To examine the consequence of functional gain of TWK-40, we engineered a missense mutation at a conserved amino acid (L181N) known to increase K2P channel's conductance by reducing the hydrophobic barrier inside the pore[11,12], at the endogenous

twk-40 locus (Fig. 2A; Fig. 1S–1A). In contrast to *twk-40(lf)*, this predicted gain-of-function (*gf*) lesion decreases the overall motor activity: *twk-40(gf* mutants exhibit drastically reduced forward movement and do not reverse (Fig. 1C, D). Our findings together with a report of a genetic study[13] on K2P gene manipulation, imply a genetic perturbation of a channel's activity can serve as a tool to dissect the neural circuits controlling behaviours.

Three classes of interneurons most abundantly express TWK-40

To identify cells that express TWK-40, we inserted a fluorescent reporter (tagRFP) into the endogenous *twk-40* locus to label all predicted TWK-40 isoforms (Fig. 1S–2A). This tag does not impair TWK-40's function because the engineered animals exhibit wildtype motor activity (Fig. 1S–2B).

We found that endogenous TWK-40::tagRFP was most strongly expressed in three neuron classes, AVA, AVB and DVA, with AVA expression significantly higher than the rest. TWK-40::tagRFP signals were weaker in the soma and enriched along neurites (Fig. 1B). A transgene that consists of multiple copies of a functional fosmid TWK-40::GFP reporter confirmed the endogenous TWK-40::tagRFP pattern, but revealed expression in more neuron classes, likely due to over-expression. AVA, AVB, and DVA again exhibited the strongest expression. Weak but consistent TWK-40::GFP signals were detected in 15 additional neuron classes, including interneurons (AVE, AVG, RIA, RIF, ALA, DVC, RIV), motor neurons (DA, DB, VA, VB, SAB, SIA, SIB) and sensory neurons (ALN) neurons (Fig. 1S–1B).

AVA and AVB are the descending premotor interneurons that make synaptic input to motor neurons that generate backward and forward movement, respectively. DVA is an ascending interneuron that make synaptic connections with other interneurons. A restricted TWK-40 expression favors the possibility that small changes to several core neurons can significantly alter the overall motor activity.

AVA-specific manipulation of TWK-40 regulates both forward and backward locomotion

To evaluate the functional contribution of TWK-40 expressing neurons, we first examined the effect of systemic degradation of TWK-40 from subgroups of neurons in wildtype animals. Depletion of the TWK-40 channel from neurons that critically regulate the motor activity should lead to the same phenotype as *twk-40(lf)* mutants.

We degraded endogenous TWK-40 proteins from sub-groups of TWK-40-expressing neurons using a modified ubiquitin-ligase system. Remarkably, we found that depleting TWK-40 from AVA neurons alone is sufficient for a wildtype animal to recapitulate *twk-40(lf)* mutant's overall increased motor activity ((Fig. 1C, D, Fig. 1S–2C). Notably, we did not observe similar requirement or sufficiency for AVB, AVE, DVA or other *twk-40* expressing neurons (Fig. 1S–2C). Thus, the increased motor activity in *twk-40(lf)* mutants results mainly from its effect on AVA, consistent with the higher expression of TWK-40 in AVA. Conversely, when we exogenously but specifically expressed TWK-40(gf) in AVA in wildtype animals, it was sufficient to reduce overall motor activity. Similar to *twk-40(gf)* mutants, the AVA-specific TWK-40(gf) animals had drastically reduced forward movement with shallow body bends and no backward movement altogether (Fig. 1C,D).

When we exogenously restored TWK-40 expression specifically to AVA in *twk-40(lf)* mutants, the animal's increased motor activity was rescued, with a restoration of body bending (forward and backward) to the wildtype level (Fig. 1E).

These findings indicate that AVA interneurons might be the key regulator of both backward and forward locomotion, implying that existing reciprocal inhibition model for the coordination of forward and backward motor subcircuits (Fig. 1A) may need to be modified.

AVA's RMP and activity is regulated by TWK-40, a bona fide K2P channel

To address how the AVA neurons regulate overall motor activity, we begin by asking whether TWK-40 forms a functional K^+ leak channel to regulate AVA's membrane potential.

First, we examined TWK-40's sufficiency to form a functional channel in the exogenous mammalian cell line. Expressing the wildtype and TWK-40(gf) proteins in HEK293T cells led to a small and large increase of the host cell's outward leak current, respectively (Fig. 2B). A small leak current is characteristic of an exogenously reconstituted wildtype K2P channel. A huge increased current by TWK-40(gf) is consistent with this amino acid substitution reducing the pore's hydrophobic barrier[11,12]. Decreasing intracellular K^+ dramatically reduced the currents when TWK-40(gf) was expressed. These regulates demonstrate TWK-40 constitutes a voltage-insensitive K^+ selective ion channel, in accordance with the characteristics of a functional K2P channel[14]. Consistent with the fact that K2P is a membrane protein, endogenously expressed TWK-40 protein is present at the plasma membrane of neurons (Fig. 2C). Next, we examined TWK-40's role in regulating the membrane properties of AVA by *in situ* whole-cell patch-clamp recording in an open *C. elegans* preparation. Consistent with TWK-40 forming a functional K^+ leak channel, the AVA neurons' outward current was reduced in *twk-40(lf)* and increased in *twk-40(gf)* mutant animals (Fig. 2D). In *twk-40(lf)* mutants, the leak current was restored to wildtype level with TWK-40 protein specifically expressed in AVA neurons (Fig. 2D).

As expected from reduced or increased outward leak current, AVA's RMP became further depolarized in *twk-40(lf)* mutants and hyperpolarized in *twk-40(gf)* mutants (Fig. 2E). These changes, which are expected to increase and decrease AVA's excitability, positively correlated with changes of their calcium signals in freely moving animals. In the absence of TWK-40, AVA exhibited higher fluorescence intensity for the genetic calcium sensor (GCaMP6). Consistent with increased reversal frequency and duration (Fig. 1C,D), the calcium transients in these animals were more frequent and sustained for a longer duration (Fig. 2F). In the presence of TWK-40(GF), AVA exhibited significantly lower GCaMP signals with fewer calcium transients (Fig. 2F). Together, these results show TWK-40 regulates AVA's RMP and membrane excitability.

Consistent with previous reports[8,9], we found that in wildtype animals, AVA's RMP ranged between -20mV to -27mV (Fig. 2E), which is unusually depolarized compared to other recorded neurons (Fig. S2A shows AVB RMP)[15–26], summarized in Supplemental Table 1). In *twk-40(lf)* mutants, AVA's RMP was further depolarized, lying between -21mV to -15mV (Fig. 2E). While, in *twk-40(gf)* mutants, it was more hyperpolarized, lying between -25mV to -55mV (Fig. 2E). Such unusually depolarized RMP cannot be simply explained by recording conditions for the *C. elegans* preparation.

In summary, by characterization of TWK-40, we demonstrated that a more depolarized AVA's RMP in *twk-40(lf)* mutants leads to an increased activity in both forward and backward motor states. While more hyperpolarized AVA's RMP in *twk-40(gf)* mutants decreases activity of both motor states, suggesting that AVA's unusually depolarized RMP might be the key to its coordination of both forward and backward motor subcircuits.

The 'backward' premotor interneuron AVA potentiates forward locomotion and the corresponding motor subcircuit. Manipulation of AVA's RMP revealed its role in maintaining the motor activity for both forward and backward movement. This was unexpected because previous studies establish AVA as the regulator of the subcircuit for backward locomotion. Because of the antagonizing nature of the forward and backward motor states, AVA's effect on the forward motor state could be considered a consequence of the reciprocal inhibition from AVB[6].

To examine whether AVA neurons play a direct role during forward movement, we removed the sub-circuit that generates backward movement. We expressed a light-inducible singlet oxygen generator miniSOG in the A class reversal motor neurons, to induce cell death in live animals[3,27]. Ablation of A motor neurons did not cause significant changes to the forward movement (Fig. S3A). In this background, we further ablated AVA through AVA-specific expression of miniSOG. Upon AVA ablation, the animal's forward movement was significantly attenuated, with reduced body bends and velocity (Fig. 3A). In*twk-40(lf)* mutants, ablation of AVA/A similarly reduced the forward speed and curvature (Fig. 3A). These results show that AVA neurons are required to sustain forward locomotion.

We further examined whether this effect is specific to RMP-induced AVA activity change. AVA neurons are electrically coupled with other neurons, including the A class motor neurons that execute backward movement[28]. Coupling between AVA and A requires an innexin UNC-7[28], and UNC-7-dependent coupling shunts spontaneous reversals[2]. In *unc-7(lf)* mutants, AVA's exhibit a decreased membrane capacitance without altered RMP[2], resulting in increased excitability and calcium activity[2,3].

UNC-7 is expressed by multiple neurons[2,3]. We performed AVA-specific UNC-7 depletion in animals where the backward motor circuit has been silenced. AVA-specific UNC-7(lf) led to significant increase of AVA's calcium activity (Fig. S3B). To text whether such RMP-independent increased activity alter forward locomotion, we examined the forward locomotion in AVA-specific UNC-7(lf) animals with reversal A motor neuron silenced. These animals exhibited increased curvature (Fig. 3C (i)), with no apparent change in velocity (Fig. 3C). AVA activity increase due to gap junction uncoupling also led to an increase of curvature in AVA-specific TWK-40(gf) animals (Fig. 3C (ii)). Thus, similar to AVA-specific TWK-40(lf), AVA-specific UNC-7(lf) also potentiates forward movement.

Regardless of how we perturbed AVA's activity, the change in animal's forward movement corresponded with the change in forward motor circuit activity. In different genetic backgrounds, calcium activity of forward motor-neurons VB10 and DB4 changed in correspondence to their locomotor patterns. Both motor neurons showed an increased activity in AVA-specific TWK-40(lf) and AVA-specific UNC-7(lf) animals, while VB10 activity decreased in AVA-specific TWK-40(gf) animals (Fig. 3B, D).

These results reveal that the activity of AVA neurons is required to maintain the activity of the forward motor circuit, which is independent of their regulation on the reversal state.

AVA's chemical synaptic transmission underlies its regulation of forward movement

AVA neurons could potentiate the forward movement through chemical or electrical synapses. In *unc-7(lf)* and AVA-UNC-7(lf) innexin mutants, AVA neurons exhibit increased activity, leading to increased forward movement. Thus, AVAs's potentiation of forward motor movement may not be fully dependent on electrical synapses.

To address whether the potentiation of forward locomotion requires chemical transmission, we examined the effect of blocking AVA's chemical transmission using tetanus toxin light chain (TeTx), likely neurotransmission specific (Methods). AVA-specific TeTx animals exhibited reduced, but not diminished, forward and backward motor activity (Fig. 4A, Fig. S4A). Specifically, their velocity and curvature were reduced during forward movement. In *twk-40(lf)* mutants, AVA-specific TeTx also led to strong reduction of forward velocity and a mild but significant reduction of curvature during forward movement (Fig. 4A). Consistent with their behavioral changes, the forward B motor neurons also exhibited reduced calcium activity in AVA-specific-TeTx animals (Fig. 4B). These results suggest that chemical transmission from AVA plays a critical role in potentiating forward movement.

Chemical transmission may occur through classical neurotransmitters, monoamines, or neuropeptides. AVAs are cholinergic neurons and synthesize multiple neuropeptides[29,30]. We blocked cholinergic transmission from AVA to investigate whether it potentiates the forward locomotion through classical neurotransmitters. Using AVA-specific RNA interference (RNAi), we reduced the loading of acetylcholine into synaptic vesicles in AVA by *cha-1* RNAi. This led to a similar degree of reduction in forward velocity and curvature as that of AVA-specific TeTx (Fig. S4B). These results reinforce that AVA's potentiation of forward movement requires cholinergic synaptic transmission.

AVA's potentiation of forward locomotion requires AVB

To address which components of the forward motor subcircuit mediate AVA's potentiation of forward locomotion, we performed genetic ablation of several individual neurons involved in forward locomotion. We found that ablation of AVB in wildtype, AVA-

specific TWK-40(lf) and AVA-specific TWK-40(gf) animals. Consistent with previous findings[4], ablation of AVB in wildtype animals led to significantly reduced forward speed and curvature (Fig. 5A). Similarly, ablating AVB in AVA-specific TWK-40(lf) animals reduced their forward speed and curvature (Fig. 5B). While, ablation of AVB in AVA-specific TWK-40(gf) animals did not exacerbate their reduced curvature or velocity (Fig. S5A).

To further examine the relationship between AVA and AVB, we examined the calcium activity of AVB upon manipulation of AVA's activity. In AVA-specific TWK-40(lf) animals, AVB calcium activity was increased during forward movement (Fig. 5C). Similar increase was found in AVA-specific UNC-7(lf) animals (Fig. S5B). While, in AVA-specific TWK-40(gf) animals, AVB calcium activity was reduced significantly (Fig. 5C). Together, these results indicate that AVA's potentiation of forward locomotion occurs mainly through AVB premotor interneurons. This is surprising given the fact that AVA does not form electrical or chemical synapses with AVB or B-class forward motor neurons[5,7].

Acute optogenetic hyperpolarization of AVA inhibits both forward and backward movement

To further examine AVA's regulation of forward and backward locomotion we resorted to optogenetics. First, we used GtACR2, a light-activated anion opsin to silence AVA's activity. We found GtACR's effect to be extremely potent: even with minimal light intensity, its activation instantaneously immobilized the animal regardless of the motor state prior to stimulation (Fig. S6C, strong activation). The effect of strong activation, where AVA-GtACR2 induced instantaneous full body immobilization, could not be reversed by either AVA-specific TeTx or AVA-specific UNC-7(lf) (Fig. S6C). We can only speculate that this phenotype is non-physiological, likely induced by a decrease of AVA's membrane potential beyond their physiological range during forward and backward movement. This motivated us to develop a new stimulation protocol with a dramatic reduction of all-trans retinal (ATR) on the imaging plates (Methods). With this protocol, the minimal light stimulation of AVA-specific GtACR2 mimicked AVA-specific TWK-40(gf) animals, with abolished backward movement and reduced forward movement (Fig. 6A; Fig. S6D, weak activation).

Next, we further examined the dependence of AVA's chemical and electric transmission on forward locomotion. Similar to AVA-specific TWK-40(gf) animals, and as expected, blocking AVA's chemical synaptic transmission by TeTx did not further reduce the forward movement of AVA-specific GtACR2 animals (Fig. 6A and S6D). In contrast, AVA-specific UNC-7(lf) abolished GtACR2-mediated attenuation of the forward movement (Fig. 6A; S6D). Consistent with a requirement of AVB for AVA's effect on forward movement, ablation of AVB significantly attenuated, although did not abolish the GtACR2-mediated inhibition of the forward movement (Fig. 6B). These results indicate that optogenetic hyperpolarization of AVA mimics AVA-specific TWK-40(gf). Further, the attenuation of forward movement occurs mainly through UNC-7 mediated electric coupling.

Phasic and tonic optogenetic stimulation of AVA activates backward and forward movement

AVA's potentiation of forward locomotion is in direct opposition to several previous observations that rapid, phasic optogenetic stimulation of AVA causes animals to move backward. The phasic effect of AVA on backward movement is likely neurotransmission dependent, as AVA-TeTx attenuates the backward movement in AVA phasic activated animals (Fig. S6A) . To reconcile these results we developed different optogenetic stimulation protocols. Surprisingly, we found that a tonic and weak stimulation protocol of AVA, which involved pre-exposing AVA-Chrimson (a red shift channelrhodopsin) animals to green light (between 3-5 minutes) on very low concentration ATR plates (Methods), caused them to phenocopy AVA-specific TWK-40(lf) animals (Fig. 6C(i), pre-exp +ATR). Specifically, the tonic and weak stimulation protocol induced more frequent transitions between forward and backward motor movement, with increased bending during not only backward but also forward movements. Weak optogenetic stimulation of AVA, with no pre-exposure, preferentially activated reversals, without affecting their forward motor state (Fig. 6C(i), no-pre-exp +ATR). This means that tonic activation of AVA is crucial for the potentiation of forward locomotion.

We have shown that AVA's potentiation of forward movement is dependent on their chemical transmission and AVB premotor interneurons. Consistent with this, we found that tonic optogenetic stimulation induced potentiation of forward locomotion was abolished by AVA-specific TeTx (Fig. 6C(ii)) and upon AVB ablation (Fig. 6D).

These experiments consolidate our findings that the 'backward' premotor interneuron AVA regulates both forward and backward locomotion in *C. elegans*. Additionally, these data revealed that AVA's effect on the two motor subcircuits is likely organized at two different time-scales. Consistent with previous reports, we find that AVA leads to backward locomotion via rapid, phasic stimulation. While AVA's potentiation of forward locomotion occurs through tonic excitation of the forward motor subcircuit, likely via AVB premotor interneurons.

Discussion

TWK-40 antagonized sodium leak conductance's effect on AVA's activity

Two functionally antagonistic conductance - outward potassium current and inward sodium current - exerts opposite effects on a neuron's RMP. Previously, we showed that genes encoding the Na^+ leak channels, NCA, are expressed broadly in the nervous system, but functions cell autonomously to establish AVA's depolarized RMP[8,31]. *nca-1(gf)* mutant animals exhibited increased curvature during both forward and backward movement and increased backward propensity (Fig. S2B (i, ii, iii), a motor pattern superficially similar to *twk-40(lf)*, in agreement with the notion that gain-of-function of NCA depolarizes the RMP and likely increases the activity of most neurons. Further, we found that *twk-40(gf)* led to partial restoration of forward and backward locomotion in *nca(gf)* animals (Fig 2SB), which is consistent with a recent genetic study[13]. Furthermore, an increased and restored AVA calcium activity in *nca(gf)* and in *twk-40(gf); nca(gf)* animals are corresponding to their locomotion changes(Fig. 2SC).

These results support that AVA premotor interneurons activity likely contribute the locomotion in *nca-1(gf)* and *twk-40(gf); nca-1(gf)* animals.

AVA is a master neuron for forward and backward movement

At the level of motor neurons, *C. elegans* motor circuits function largely independently during forward and backward locomotion. Ablating forward motor neurons has minimal effect on backward locomotion, while ablating backward motor neurons has minimal effect on forward locomotion[3]. It is commonly assumed that this functional independence is maintained even at the level of premotor interneurons, for example via reciprocal inhibition between AVA and AVB premotor interneurons[6].

Our study shows that this view does not completely capture the premotor interneuron regulation of forward and backward motor circuits. Crucially, at the level of premotor interneurons, the two circuits are not independent. In particular, lowering the activity of the reversal premotor interneuron, AVA, in different ways reduces the overall locomotor activity of *C. elegans*, suggesting that AVA serves as a master neuron, promoting both forward and backward locomotion.

A phasic-tonic model for AVA's regulation of motor states

Based on our experimental findings, we can propose a new functional model for premotor interneuron regulation of *C. elegans* motor circuits, which is schematically shown in 7. Like previous models, we propose that rapid, phasic activation of AVA induces and maintains backward locomotion. In addition, we claim that due to its unusually depolarized RMP, AVA is likely constitutively active. Even in its low-activity state, it promotes forward locomotion by positively regulating AVB's activity through tonic release of acetylcholine. This phasic-tonic model of AVA's regulation of *C. elegans* motor circuits, exemplified by opposing effects of phasic and tonic optogenetic stimulation of AVA, neatly consolidates the AVA-specific TWK-40(lf) and AVA-specific TWK-40(gf) phenotypes and reconciles them with seemingly contradictory results from previous studies. Further experiment and computational modeling will be applied to consolidate the findings.

Notably, our functional model cannot be simply explained by anatomical wiring in *C. elegans*. In particular, AVA makes no electrical or chemical synapses with AVB motor neurons. This suggests that AVA's effect on AVB's activity might be indirect through intermediate neurons or through extrasynaptic mechanisms, similar to the extrasynaptic activation of the ventral motor subcircuit in the L1 larva[32].

Methods

Constructs and strains

See Supplemental Table 2 for a full list of constructs and stains generated and used in this study. *unc-7::AID (zwIs 141)* is a gift from Zhaowen Wang. Primers and sequences are available upon request. All *C. elegans* strains were cultured on the standard Nematode Growth Medium (NGM) plates seeded with OP50, and maintained at 22 °C unless specified. The wildtype animal refers to the Bristol N2 strain. Hermaphrodite worms were used for the experiments. Promoter: *twk-40*(1.5k before ATG of T28A8.1b).

Isolation, cloning and generation of *twk-40* mutants

Loss-of-function allele *twk-40 (hp834)* was a 7bp deletion at base 3378-3384 (GTTCGAG) of T28A8.1b generated by CRISPR/Cas9 genome editing.

Gain-of-function allele *twk-40 (bln336, L181N*) was engineered by CRISPR/Cas9 system by mutating 4298-4299 base of T28A8.1b from CT to AA.

TWK-40 degradation was generated by a repurposed E3 ligase degradation system. Specifically, *bln282 (twk-40::tagRFP::ZF)* was generated by CRISPR/Cas9 genome editing to insert an inframe tagRFP::ZF fusion at basepair 5785 at T28A8.1b (twk-40)[33]. By exogenously expression of ZIF-1 under different promoter allows cell specific TWK-40 degradation.

AVA-specific TWK-40(lf) was generated by expressing ZIF in AVA using *rig-3* promoter or *nmr-1*/*rig-3*-promoter combination (*Prig-3 FRT zif-1 sl2 eBFP FRT; Pnmr-1-FLP*) via FRT/FLP recombination system in *bln282 (twk-40::tagRFP::ZF)* background. AVA-specific TWK-40(gf) was generated by expressing TWK-40(L181N)::GFP in AVA by *flp-18*/*twk-40*-promoter combination (*Pflp-18-loxp stop loxp twk-40(gf)::GFP; Ptwk-40-cre*) or via Cre/loxp recombination system in N2 background, or *rig-3*/*nmr-1* promoter combination (*Prig-3-loxp stop loxp twk-40(gf)::GFP; Pnmr-1-cre*) via FRT/FLP recombination system in N2 background. AVA-specific TWK-40 rescue was generated by expressing TWK-40(WT)::GFP in AVA by *rig-3*/*nmr-1*-promoter combination (*Prig-3 FRT Stop FRT twk-40::GFP; Pnmr-1-FLP*) via Cre/loxp recombination system in twk-40(lf) background animals.

Locomotion assay

A single L4 animal was collected and transferred to an NGM plate with a thin layer of OP50. After 30 seconds, it was recorded on a tracking microscope using an in-house developed ImageJ plugin. A 3-minute movie of the animals was recorded at 10 fps. At least 10 animals for each genotype were recorded on the same day using the same condition. The movies were analyzed as previous published[2]. Only the absolute value of body curvature was calculated in this study (segments 5-32 out of 33). Velocity was calculated by the centroid shift of the animals.

Immunofluoresent staining

Mixed stages of animals of twk-40::tagRFP::ZF (for determining cell expression) and twk-40::tagRFP::ZF; pref-1-GPI::YFP were fixed in 2 percent paraformaldehyde at 4°C for 1 hour and processed as previously described[34,35] . Primary antibodies against tagRFP (Thermo Fisher Scientific, R10367, rabbit) and GFP (Roche, mouse) were used at 1:500 and 1:200 dilution, respectively.

A secondary antibody of goat-anti-rabbit (Alexa Fluor 488) and goat anti-mouse (Alexa Fluor 594) was used at 1:5000 dilution. L4 stage larva and adults were imaged with a Nikon spinning disk confocal microscope with a 63x objective and reconstructed by maximum intensity projection. Single layers of acquired images from animals co-expressing TWK-40::tagRFP::ZF and GPI::YFP were examined for subcellular colocalization using an ImageJ plugin (JACoP) and Pearson's coefficient is calculated between GFP and RFP signals.

Electrophysiology

HEK293 cell expression and electrophysiology recording: HEK293 cells culture conditions include DMEM medium, 10 percent fetal bovine serum, 1 percent double antibody, 5 percent CO2 and 37 °C. TWK-40 cDNA was flanked between BstXI and NheI sites by PCR and cloned into the pCDNA3.1 vector. Transfection and expression of plasmid in HEK293 cells by liposome ExFect2000 (Vazyme, China). After 24 hr, HEK293 cells were patched using 4–6 MΩ-resistant borosilicate pipettes (1B100F-4, World Precision Instruments, USA). Pipettes were pulled by micropipette puller P-1000 (Sutter, USA), and fire-polished by microforge MF-830 (Narishige, Japan). Membrane potential and I-V curve were recorded in the whole-cell configuration by EPC-9 amplifier (HEKA, Germany), using the pulse and processed with Igor Pro (WaveMetrics, USA) and Clampfit 10 software (Axon Instruments, Molecular Devices, USA). Membrane potential was recorded at 0 pA, I-V curve was recorded at holding potential from –80 mV to 80mV. Data were digitized at 10–20 kHz and filtered at 2.6 kHz. The pipette solution contains (in mM): KCl 140; MgCl2 1; EGTA 10; HEPES 10; Na2ATP 4; pH 7.3 with KOH, 300 mOsm. The bath solution consists of (in mM): NaCl 140; KCl 3.6; CaCl2 2.5; MgCl2 1; pH 7.3 with NaOH, 310 mOsm. For low intracellular K+ recording, the pipette solution contains (in mM): KCl 14; CsCl 126; MgCl2 1; EGTA 10; HEPES 10; Na2ATP 4; pH 7.3 with KOH, 300 mOsm. Chemicals were obtained from Sigma unless stated otherwise. Experiments were performed at room temperatures (20–22 °C).

in-situ whole-cell patch clamp: Premotor interneurons AVA whole cell patch clamp was performed as previously described[2] which was modified from refs[9,36]. Premotor interneurons AVB: briefly, 1- or 2-day-old hermaphrodite adults were glued (Histoacryl Blue, Braun) to a sylgard-coated cover glass covered with bath solution (Sylgard 184, Dowcorning) under a stereoscopic microscope (M50, Leica). After clearing the viscera by suction through a glass pipette, the cuticle flap was turned and gently glued down using WORMGLU (GluStitch Inc.) to expose the AVB neurons with GFP marker. Neurons were patched using 20 MΩ-resistant borosilicate pipettes (1B100F-4; World Precision Instruments). Pipettes were pulled by micropipette puller P-1000 (Sutter), and fire-polished by microforge MF-830 (Narishige). Resting membrane potential were collected in the whole-cell configuration by pulse software with EPC9 amplifier (HEKA, Germany). Potential were recorded at a holding current of 0 pA. Data were digitized at 10 kHz and filtered at 2.6 kHz. The recording pipette solution consisted of: KCl 25 mM; K-Gluconate115 mM; CaCl2 0.1 mM; MgCl2 5 mM; BAPTA 1 mM; HEPES 10 mM; Na2ATP 5 mM; Na2GTP 0.5 mM; cAMP 0.5 mM;cGMP 0.5 mM, pH 7.2 with KOH, 320 mOsm. The bath solution consisted of KCl 5 mM; NaCl 150 mM; CaCl2 5 mM; MgCl2 1 mM; glucose 10 mM; sucrose 5 mM; HEPES 15 mM, pH 7.3 with NaOH, 330 mOsm. Chemicals and blockers were obtained from Sigma unless stated otherwise. Each animal was recorded for at least 5 minutes. Experiments were performed at room temperatures (20-22 °C).

Free-moving calcium imaging and post analysis

AVA or AVB single neuron imaging was performed in L4 stage animals as previously described[37]. B motor neuron imaging: An individual transgenic animal was placed on 2.5 percent agarose gel, to ensure its slow movement. The animal was allowed to recover for 3min and then recorded using Zeiss Axioskop 2 Plus upright microscope with 40x objective (VB10) or Nikon spinning disc confocal with 20x objective (DB4). A single plane was imaged and recorded by manual tracking and refocusing. DB4 and VB10 were selected for recording because their soma position made them easy to identify. GCaMP activity (GCaMP/RFP ratio unless stated otherwise) was obtained as previously described[32].

MiniSOG cell ablation

AVA-specific miniSOG generated by expressing miniSOG sl2 mcherry in AVA by *flp-18*/*twk-40*-promoter combination (*Pflp-18-loxp stop loxp mito::miniSOG sl2 mcherry; ptwk-40-cre*) AVB, RIM, AVA, A and AVA/A ablation were performed in L2. Animals were treated by 30-40 min LED blue light and recovered for 1 day. L4 animals were recorded for behaviour. The effiency of cell ablation was examined by the disformation or disappearance of mcherry signal

Only healthy worms were recorded and analyzed. The ablation efficiency was confirmed by disappearance or distortion of the soma fluorescence and fragmentation of neurites.

Cell-specific neurotransmission block

AVA-specific expression of tetanus toxic light chain: AVA-specific TeTx animals were generated by expressing TeTx in AVA by *flp-18*/*twk-40* promoter combination (*Pflp-18-loxp Stop loxp TeTx::cherry; ptwk-40-cre*) via Cre/loxp recombination system.

In order to assess whether TeTx impair neuropeptide secretion in *C. elegans* neurons , we directly examined the effect of TeTx on neuropeptide secretion, which has remained unclear in *C. elegans*, using two markers for dense-core vesicles fusion: INS-22::GFP and INS-22::pHluorin[37–39], both being exogenously expressed in AVA (Fig. S4D).

Images of fluorescently tagged proteins were captured in live L4 worms or immunostained animals. Live worms were immobilized with dry agarose pad in M9 buffer. Fluorescence signals were captured using Nikon Eclipse 90i confocal microscope and Nikon Eclipse T12 with Yokogawa CSU-X1 spinning disk field scanning confocal system.

Both markers showed clustered signals along the AVA axons (Fig. S4D). Similar to other peptidergic markers[37], fluorescence signals also accumulated in coelomocytes (Fig. S4C), cells that phagocytose secreted molecules[40]. For the INS-22::GFP marker,

in the presence of TeTx, we observed no reduction for signals in coelomocytes and a very mild increase of signals along the neurite (Fig. S4C). With the INS-22::pHluorin, which allowed visualization of exocytosis of dense-core vesicle, we observed no difference in the steady stage florescence along AVA's neurite between wildtype and AVA-TeTx animals (Fig. S4D). Our results suggest TeTx is unlikely impair the neuropeptide secretion.

AVA-specific *cha-1* RNA interference: AVA-specific *cha-1* RNAi was generated using the *flp-18*/*twk-40* promoter combination to drive the sense and anti-sense strand of *cha-1* genomic DNA, respectively. The following primers and templates were used:

A. P*flp-18*: OZM6199, GATGGATACGCTAACAACTTGG and OZM6200, CTACAACGGCAGCGTATTCGATCCCGTCTAACCCTGAAA, amplified from pJH4631.

B. *cha-1* exon: OZM6201, GAATACGCTGCCGTTGTAG, and OZM6240, GTCGAGTGCTCTATGCACAACC, amplified from N2 genomic DNA.

C. P*twk-40*: OZM6199, GATGGATACGCTAACAACTTGG and OZM6253, GTATGATGCGACTATTCAGCTGTGAATATTCATCACTCGATATTCCA, amplified from pJH4608.

D. *cha-1* exon: OZM6201, GAATACGCTGCCGTTGTAG and OZM6202, CAGCTGAATAGTCGCATCATAC, from N2 genomic DNA.

PCR fusion was performed to obtain sense and anti-sense cha-1 by following primers: P*flp-18-cha-1*(sense): OZM6203, AGCTTAGCCGGAATAGGGTCA and OZM6202, CAGCTGAATAGTCGCATCATAC, amplified from PCR product A+B. P*twk-40-cha-1*(antisense): OZM3543, AATGCGGCCGCTCTAATCACTATCACGT GGGATCTGGATAA; OZM6254, CGTAGGCCAGAAAGCCTCAC, from PCR product C+D.

Mixed PCR products were injected into N2 animals.

Optogenetic strains and stimulation

AVA specific Chrimson and GtACR2 were generated by promoter combination via Cre/loxp system. The specificity of AVA GtACR2 was examined by ablation using *pnmr-1-miniSOG*. The AVA ablated animal no longer exhibited locomotry inhibition during forward and backward movement. Transgenic animals were cultured on ATR plates in the dark for two generations. Second-generation L4-stage animals were analyzed for behavior and calcium activities.

Behaviors upon stimulation: An individual L4-stage animal was transferred to an imaging plate with a thin layer of evenly spread OP50. After 30 seconds, the movement of the animal was tracked during multiple programmed stimulation cycles: 10s pre-stimulation, 10s stimulation, 10s post-stimulation; or, 30s pre-stimulation, 30s stimulation, 30s post-stimulation. 488nm and 574nm LED light stimulation was applied to inhibit and activate AVA, through activating GtACR2 and Chrimson, respectively.

phasic activation and strong inhibition: NGM plates were seeded with OP50/ATR mixture (1ml OP50 /5ul 50uM ATR). Animals were cultured on such plates for at least one day for behavior recording. During stimulation, animals were exposed to 595nm yellow LED light (Thorlabs, Chrimson mediated-optogenetic activation) at maximum intensity (63 out of 63 A.U.) or 470nm blue LED light (Thorlabs, GtACR2-mediated optogenetic inhibition) at maximum intensity (63 out of 63 A.U.).

Tonic and weak activation: NGM plates were seeded with OP50/ATR mixture (1ml OP50/0.5ul 50uM ATR). Animals were cultured on such plates for at least 1 day for behavior recording. Before recording, animals were treated with 544nm green LED light for 3-5min (Zeiss V16) and followed by 595nm yellow light exposure (Thorlabs) at low intensity (4 out of 63 A.U.) during recording.

Weak inhibition: NGM plates were seeded with OP50/ATR mixture (1ml OP50/0.5ul 50uM ATR). Animals were cultured on such plates for at least 1 day for behavior recording. During stimulation, animals were exposed to 470nm blue LED light at low intensity(4 out of 63 A.U.).

Statistical analyses

Mann-Whitney U test were used to quantify data of box and whisker plots. Kolmogorov-Smirnov test were used to quantify data of accumulative frequency plots.

ACKNOWLEDGEMENTS

We thank Tanya Pekar, Ying Wang, Yan Li, Maria Lim and Yangning Lu for technical support and discussions; We thank open exchange of unpublished observations with the Ma and Gao groups. We Thank Zhaowen Wang for the *unc-7 zwls141* allele. Jun Meng personally thank her cat, Dahuang. This work was supported by the Canadian Institutes of Health Research Foundation Scheme 154274 (MZ) and European Research Council (ERC Starting Grant, *Kelegans*) (TB).

AUTHOR CONTRIBUTIONS

MZ, JM conceived and supervised the study; WH generated *hp834* allele; JM carried out most molecular genetic studies; SEM, MG, TB generated strains (*bln336* and *bln282*); JM generated majority of reagents and performed calcium, behavior and optogenetics experiments. JM, TA analyzed the data; BY, LLC and SB performed all electrophsiology experiments and analyzed data; JM, TA, SB and MZ wrote the paper; all authors read or edited the paper.

COMPETING INTERESTS

The authors declare no competing interests.

References

[1] Martin Chalfie et al. "The neural circuit for touch sensitivity in Caenorhabditis elegans". In: *Journal of Neuroscience* 5.4 (1985), pp. 956–964.

[2] Taizo Kawano et al. "An imbalancing act: gap junctions reduce the backward motor circuit activity to bias C. elegans for forward locomotion". In: *Neuron* 72.4 (2011), pp. 572–586.

[3] Shangbang Gao et al. "Excitatory motor neurons are local oscillators for backward locomotion". In: *Elife* 7 (2018), e29915.

[4] Tianqi Xu et al. "Descending pathway facilitates undulatory wave propagation in Caenorhabditis elegans through gap junctions". In: *Proceedings of the National Academy of Sciences* 115.19 (2018), E4493–E4502.

[5] John G White, Eileen Southgate, and J Nichol Thomson. "The structure of the nervous system of the nematode Caenorhabditis elegans". In: (1986).

[6] William M Roberts et al. "A stochastic neuronal model predicts random search behaviors at multiple spatial scales in C. elegans". In: *Elife* 5 (2016), e12572.

[7] Daniel Witvliet et al. "Connectomes across development reveal principles of brain maturation". In: *Nature* 596.7871 (2021), pp. 257–261.

[8] Lin Xie et al. "NLF-1 delivers a sodium leak channel to regulate neuronal excitability and modulate rhythmic locomotion". In: *Neuron* 77.6 (2013), pp. 1069–1082.

[9] Jerry E Mellem et al. "Action potentials contribute to neuronal signaling in C. elegans". In: *Nature neuroscience* 11.8 (2008), pp. 865–867.

[10] Seth R Taylor et al. "Molecular topography of an entire nervous system". In: *Cell* 184.16 (2021), pp. 4329–4347.

[11] Ismail Ben Soussia et al. "Mutation of a single residue promotes gating of vertebrate and invertebrate two-pore domain potassium channels". In: *Nature communications* 10.1 (2019), pp. 1–13.

[12] Prafulla Aryal et al. "A hydrophobic barrier deep within the inner pore of the TWIK-1 K2P potassium channel". In: *Nature communications* 5.1 (2014), pp. 1–9.

[13] Chuanman Zhou et al. "Differential modulation of C. elegans motor behavior by NALCN and two-pore domain potassium channels". In: *PLOS Genetics* 18.4 (2022), e1010126.

[14] Péter Enyedi and Gábor Czirják. "Molecular background of leak K+ currents: two-pore domain potassium channels". In: *Physiological reviews* 90.2 (2010), pp. 559–605.

[15] Daniel Ramot, Bronwyn L MacInnis, and Miriam B Goodman. "Bidirectional temperature-sensing by a single thermosensory neuron in C. elegans". In: *Nature neuroscience* 11.8 (2008), pp. 908–915.

[16] Miriam B Goodman and Piali Sengupta. "The extraordinary AFD thermosensor of C. elegans". In: *Pflügers Archiv-European Journal of Physiology* 470.5 (2018), pp. 839–849.

[17] Qiang Liu et al. "C. elegans AWA olfactory neurons fire calcium-mediated all-or-none action potentials". In: *Cell* 175.1 (2018), pp. 57–70.

[18] Martina Nicoletti et al. "Correction: Biophysical modeling of C. elegans neurons: Single ion currents and whole-cell dynamics of AWCon and RMD". In: *PloS one* 16.8 (2021), e0256930.

[19] Robert O'Hagan, Martin Chalfie, and Miriam B Goodman. "The MEC-4 DEG/ENaC channel of Caenorhabditis elegans touch receptor neurons transduces mechanical signals". In: *Nature neuroscience* 8.1 (2005), pp. 43–50.

[20] Miriam B Goodman et al. "Active currents regulate sensitivity and dynamic range in C. elegans neurons". In: *Neuron* 20.4 (1998), pp. 763–772.

[21] Tomomi Shindou et al. "Active propagation of dendritic electrical signals in C. elegans". In: *Scientific reports* 9.1 (2019), pp. 1–12.

[22] Shana L Geffeney et al. "DEG/ENaC but not TRP channels are the major mechanoelectrical transduction channels in a C. elegans nociceptor". In: *Neuron* 71.5 (2011), pp. 845–857.

[23] May Dobosiewicz, Qiang Liu, and Cornelia I Bargmann. "Reliability of an interneuron response depends on an integrated sensory state". In: *Elife* 8 (2019), e50566.

[24] S Faumont, TH Lindsay, and SR Lockery. "Neuronal microcircuits for decision making in C. elegans". In: *Current opinion in neurobiology* 22.4 (2012), pp. 580–591.

[25] Ping Liu, Bojun Chen, and Zhao-Wen Wang. "SLO-2 potassium channel is an important regulator of neurotransmitter release in Caenorhabditis elegans". In: *Nature communications* 5.1 (2014), pp. 1–12.

[26] Jingyuan Jiang et al. "C. elegans enteric motor neurons fire synchronized action potentials underlying the defecation motor program". In: *bioRxiv* (2021).

[27] Yingchuan B Qi et al. “Photo-inducible cell ablation in Caenorhabditis elegans using the genetically encoded singlet oxygen generating protein miniSOG”. In: *Proceedings of the National Academy of Sciences* 109.19 (2012), pp. 7499–7504.

[28] Ping Liu et al. “Antidromic-rectifying gap junctions amplify chemical transmission at functionally mixed electrical-chemical synapses”. In: *Nature communications* 8.1 (2017), pp. 1–16.

[29] Ashwani Bhardwaj et al. “FLP-18 functions through the G-protein-coupled receptors NPR-1 and NPR-4 to modulate reversal length in Caenorhabditis elegans”. In: *Journal of Neuroscience* 38.20 (2018), pp. 4641–4654.

[30] Marc Hammarlund et al. “The CeNGEN project: the complete gene expression map of an entire nervous system”. In: *Neuron* 99.3 (2018), pp. 430–433.

[31] Shangbang Gao et al. “The NCA sodium leak channel is required for persistent motor circuit activity that sustains locomotion”. In: *Nature communications* 6.1 (2015), pp. 1–11.

[32] Yangning Lu et al. “Extrasynaptic signaling enables an asymmetric juvenile motor circuit to produce a symmetric gait”. In: *Available at SSRN 3979184* (2021).

[33] Sonia El Mouridi et al. “Reliable CRISPR/Cas9 genome engineering in Caenorhabditis elegans using a single efficient sgRNA and an easily recognizable phenotype”. In: *G3: Genes, Genomes, Genetics* 7.5 (2017), pp. 1429–1437.

[34] Edward Yeh et al. “A putative cation channel, NCA-1, and a novel protein, UNC-80, transmit neuronal activity in C. elegans”. In: *PLoS biology* 6.3 (2008), e55.

[35] Jun Meng et al. “Myrf ER-bound transcription factors drive C. elegans synaptic plasticity via cleavage-dependent nuclear translocation”. In: *Developmental cell* 41.2 (2017), pp. 180–194.

[36] Janet E Richmond and Erik M Jorgensen. “One GABA and two acetylcholine receptors function at the C. elegans neuromuscular junction”. In: *Nature neuroscience* 2.9 (1999), pp. 791–797.

[37] Maria A Lim et al. “Neuroendocrine modulation sustains the C. elegans forward motor state”. In: *Elife* 5 (2016), e19887.

[38] Stacey L Edwards et al. “Impaired dense core vesicle maturation in Caenorhabditis elegans mutants lacking Rab2”. In: *Journal of Cell Biology* 186.6 (2009), pp. 881–895.

[39] Patrick Laurent et al. “Genetic dissection of neuropeptide cell biology at high and low activity in a defined sensory neuron”. In: *Proceedings of the National Academy of Sciences* 115.29 (2018), E6890–E6899.

[40] Hanna Fares and Barth Grant. “Deciphering endocytosis in Caenorhabditis elegans”. In: *Traffic* 3.1 (2002), pp. 11–19.

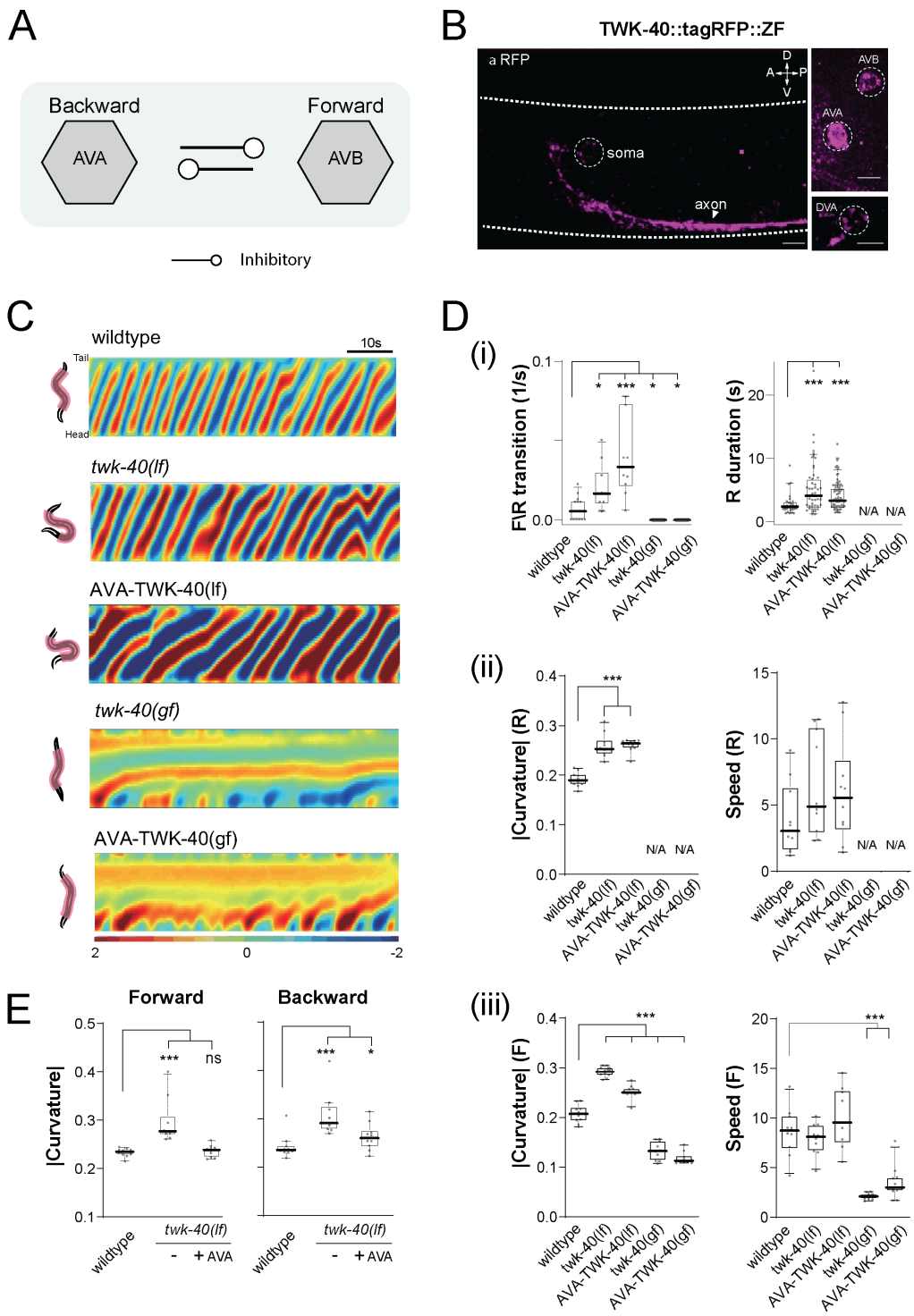

Figure 1. Premotor interneuron for backward state, AVA, regulates both forward and backward motor state through TWK-40.
A. Functional relationship between forward and backward motor states has been previously modeled with a reciprocal inhibition between AVA and AVB interneurons. **B.** Maximum projection of confocal images of immunostained endogenous TWK-40::tagRFP proteins. Left panel: the dashed lines outline the animal. AVA soma is denoted by a circle. The arrowhead labels the signal of the processes along the ventral nerve cord. Right panels: (up) AVA and AVB soma; (down) DVA soma. Scale bar, 2um. **C.** Representative heatmaps of body curvature plot of a crawling animal of each genotype (the body is highlighted on the left). *twk-40(lf) (hp834)* and AVA-TWK-40(lf) animals show increased curvature. *twk-40(gf)(bln336)* and AVA-specific TWK-40(gf) animals exhibit slow forward movement with decreased curvature. **D.** Averaged forward to backward transition frequency in each genotype. (i, Left panel) *twk-40(lf)(hp834)* and AVA-specific TWK-40(lf) have increased reversal frequency. (i, Left panel) No reversal events were detected in *twk-40(gf)(bln336)* and AVA-specific TWK-40(gf). (i, Right panel) averaged reversal duration in each genotype. *twk-40(lf)(hp834)* and AVA-specific TWK-40(lf) exhibit prolonged reverals. (i, Right panel and iii) N/A indicates the fact that no events were detected in *twk-40(gf)*. Averaged curvature (absolute value) and speed during backward (ii) and forward (iii) movement in each genotype. *twk-40(lf) (hp834)* and AVA-TWK-40(lf) animals show increased curvature during backward and forward movement. No significant changes of reversal and forward speed were detected in *twk-40(lf)* and AVA-specific TWK-40(lf) animals. *twk-40(gf)(bln336)* and AVA-specific TWK-40(gf) exhibit decreased curvature and speed during forward state. **E.** Averaged curvature (absolute value) during forward (left panel) and backward (right panel) movement in each genotype. AVA-specific TWK-40 in *twk-40(lf)(hp834)* restores its curvature to wildtype level during forward and backward movement. AVA- denotes no restored TWK-40 expression in AVA. AVA+ denotes restored TWK-40 expression in AVA.

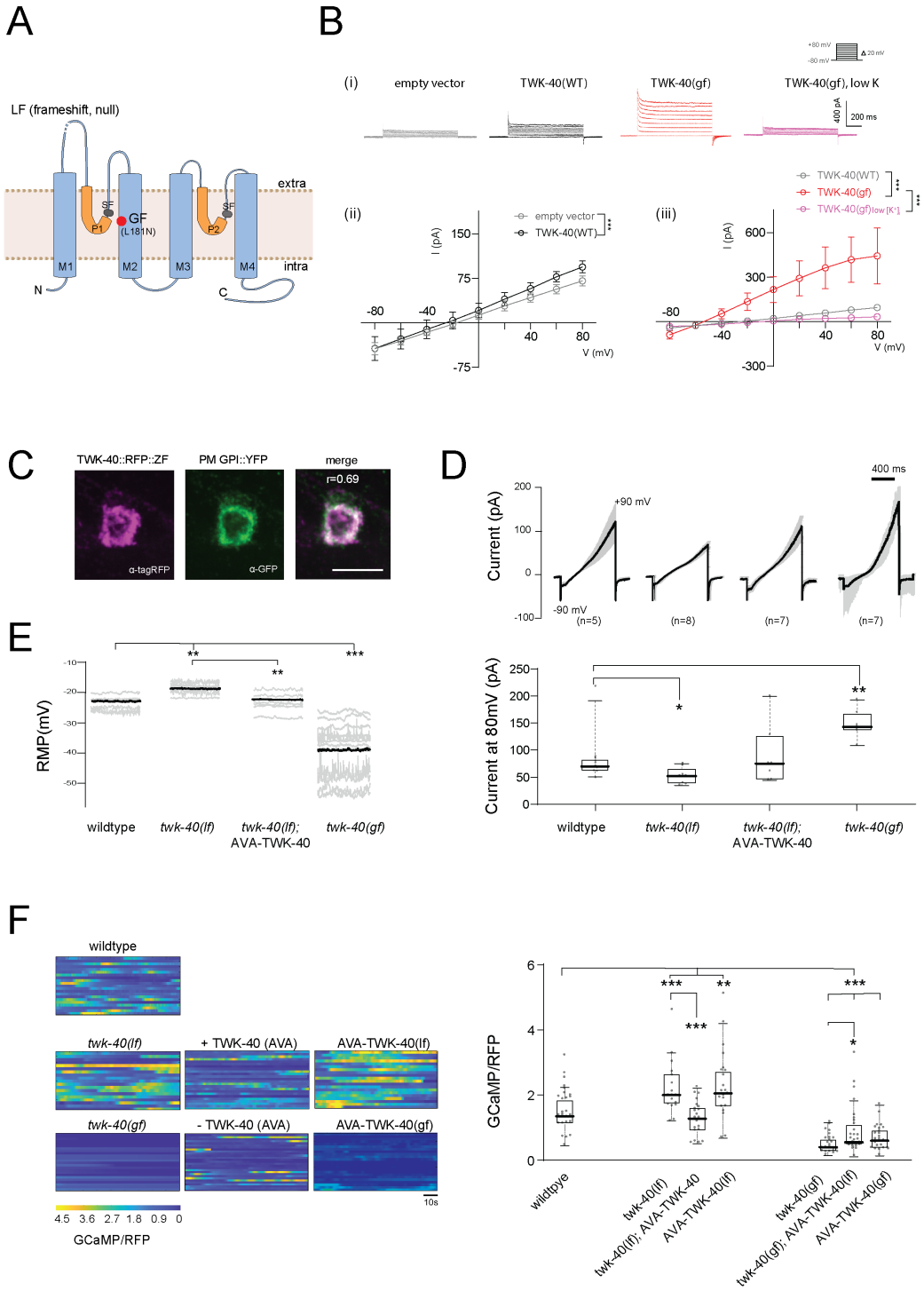

Figure 2. TWK-40, K2P, regulates RMP and neuronal excitability.

A. Illustration of the predicted topological structure of TWK-40 (isoform b) with positions of each genetic mutation annotated. LF: *hp834*, null, a 7bp exon deletion that leads to a truncation after TM1. GF: *bln336* (L181N), a point mutation inside the hydrophobic barrier of the pore domain. **B.** (Up panel)Representative step currents were recorded by whole-cell voltage-clamp from HEK293 cells with expression of different vectors. Cells were holding at -80 mV with increment of +10 mV. While mild outward currents were recorded from the cells with expression of TWK-40(WT)(Bottom left), larger currents were observed in the cells by expressing of TWK-40(GF) (Bottom right). Quantification of the current-voltage curves from different expression groups reveals that TWK-40 constitutes a functional voltage-insensitive outward channel. (Bottom right) Reloading of the intracellular K+ from 140 mM to 14 mM diminished the outward currents of TWK-40(GF). **C.** Single panel confocal images of co-staining of tagRFP and GFP in twk-40::tagRFP; pan-neuronal GPI::YFP animals. TWK-40 localizes to the plasma membrane. Pearson's correlation coefficient is shown. **D.** (Up panel) averaged traces and (bottom panel) quantification (at -80mV) of AVA's leak current in each genotype by whole-cell patching (ramp currents, holding potential is -60mV). The range of each is highlighted in grey. In *twk-40(lf) (hp834)*, the leak current is reduced and can be restored by AVA-specific TWK-40(gf) expression. Leak current is increased in *twk-40(gf) (bln336)*. The numbers of recorded animals are shown. **E.** All along the averaged traces of AVA's RMP by whole-cell patch-clamp recordings. AVA hold an averaged RMP -23mV in wildtype animals; AVA becomes more depolarized in *twk-40(lf) (hp834)*. AVA-specific restoration of TWK-40 restores its RMP to wildtype level. *twk-40(gf) (bln336)* holds a more hyperpolazied RMP of -40mV. **F.** (Left panel) raster plots and (right panel) quantification of AVA's activity in freely moving animal (GCaMP/RFP ratio) by genotypes. Each trace represents one animal. *twk-40(lf)(hp834)* exhibits increased overall activities, which is restored by the AVA-specific expression of TWK-40. AVA-specific TWK-40(lf) exhibits a similar pattern as *twk-40(lf) (hp834)*. *twk-40(gf)(bln336)* shows low activity and no obvious changes during recordings. Depletion of TWK-40(gf) from *twk-40(gf)(bln336 bln282)* in AVA partially increased AVA activity. AVA-specific TWK-40(gf) and *twk-40(gf)(bln336)* animals exhibit a similar level of AVA activity.

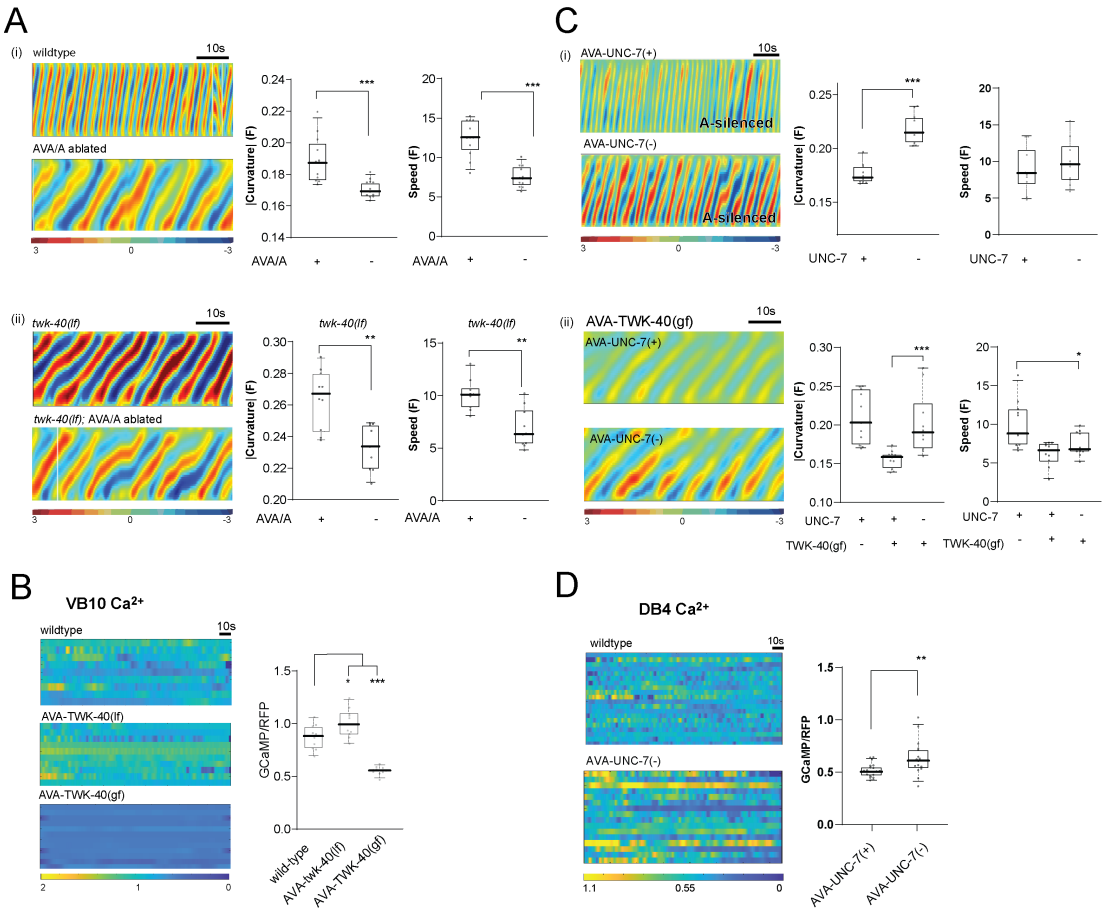

Figure 3. Genetic manipulation of AVA's activity alters forward locomotion and the activity of forward motor neurons.
A. (i,ii, left panel) a representative heatmap of curvature in control (LED non treated) and AVA-specific/A-MN co-ablated (LED treated) animals of wildtpe (i) and in *twk-40(lf)* background (ii). Averaged curvature during forward movement (i, ii, mid panel) and forward speed (i, ii, right panel) in control and AVA-specific/A-MN co-ablated animals of wildtpe (i) and *twk-40(lf)* background (ii). Co-ablation leads to a significant reduction in both curvature and speed during forward movements in both wildtype and *twk-40(lf)* background animals. **B.** (Left panel) raster plot and (right panel) quantification of VB10 activity during all motor states, represented by the GCaMP/RFP ratio in freely moving wildtype, AVA-specific TWK-40(lf) and AVA-specific TWK-40(gf) animals. Each trace represents one animal. VB10 exhibits increased and decreased activities in AVA-TWK-40(lf) and AVA-TWK-40(gf) animals, respectively. **C.** (i,ii, left panel) representative heatmap of curvature in control (Auxin non treated) and AVA-specific UNC-7(lf) (Auxin treated) animals of A-TWK-18(gf) (i) and AVA-TWK-40(gf) (ii) background; averaged curvature during forward motor state (i,ii, mid panel) and forward speed (i, ii, right panel) in each genotype . AVA-UNC-7(lf) increases forward bending in A-TWK-18(gf) and AVA-specific TWK-40(gf) background animals. **D.** (Left panel) raster plot and (right panel) quantification of DB4 activity during all motor states, represented by the GCaMP/RFP ratio in freely moving control (non Auxin treated) and AVA-specific UNC-7(lf) (Auxin treated) animals. Each trace represents one animal. DB4 exhibits increased activities when UNC-7 is degraded specifically from AVA.

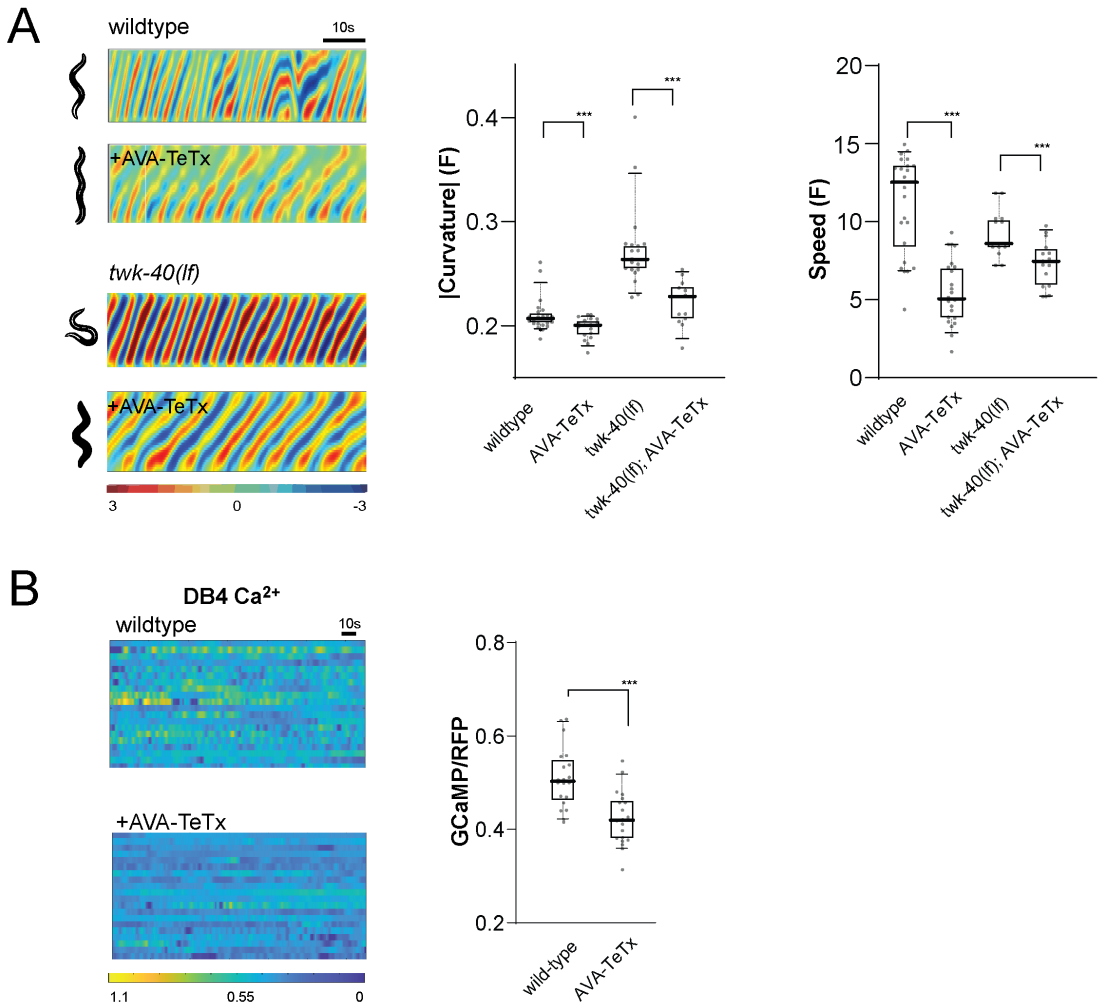

Figure 4. AVA regulates forward movement mainly through chemical synaptic transmission.
A. Representative heatmaps of the curvature (left panel), averaged curvature (mid panel) and speed (right panel) during forward movement in each genotype. Curvature during forward movement and speed are reduced in AVA-specific TeTx in both wildtype and *twk-40(lf)* background animals. **B.** Raster plot (left panel) and quantification (right panel) of DB4 activity during all motor states, represented by the GCaMP/RFP ratio in each genotype. DB4 activity is decreased in AVA-specific TeTx animals.

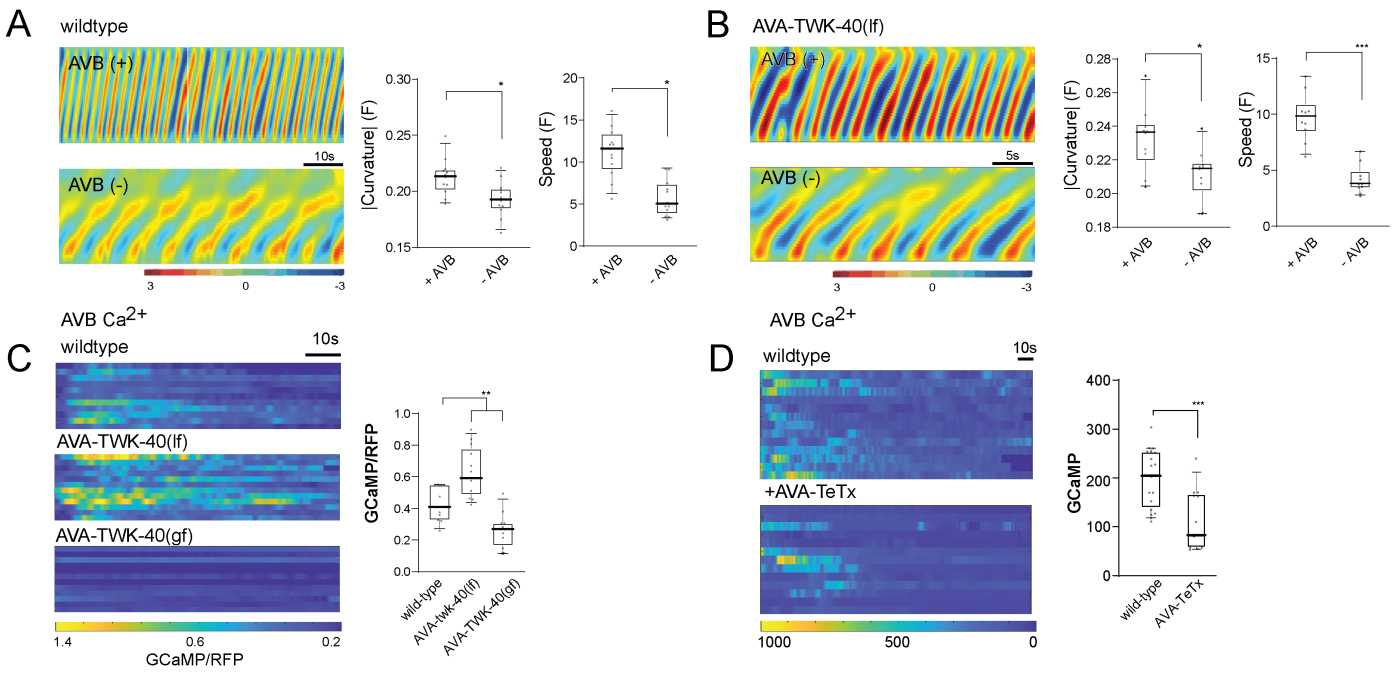

Figure 5. AVA's regulation of forward locomotion requires AVB. A (Left panel) representative heatmaps of body curvature of control (LED non treated) and AVB ablated (LED treated) animals. Averaged curvature (mid panel) and speed (right panel) during forward movement in each genotype. Ablation of AVB leads to significantly reduced forward curvature and speed. **B** (Left panel) representative heatmaps of body curvature of control (LED non treated) and AVB ablated (LED treated) animals in AVA-specific TWK-40(lf) background. Averaged curvature (mid panel) and speed (right panel) during forward movement in each genotype as in left panel. Ablation of AVB leads to significantly reduced curvature and speed in AVA-specific TWK-40(lf) animals. **C** (Left panel) raster plot and (right panel) quantification of AVB calcium activity, represented by the GCaMP/RFP ratio in freely moving wildtype, AVA-specific TWK-40(lf) and AVA-specific TWK-40(gf) animals during forward motor state. Each trace represents one animal. AVB exhibits increased and decreased activities in AVA-TWK-40(lf) and AVA-specific TWK-40(gf) animals during forward movement, respectively. **D.** (Left panel) raster plot and (right panel) quantification of AVB calcium activity during all motor states, in each genotype. Each trace represents one animal. In AVA-specific TeTx animals, AVB calcium activity is decreased . AVB calcium activity is significantly decreased in AVA-specific TeTx animals.

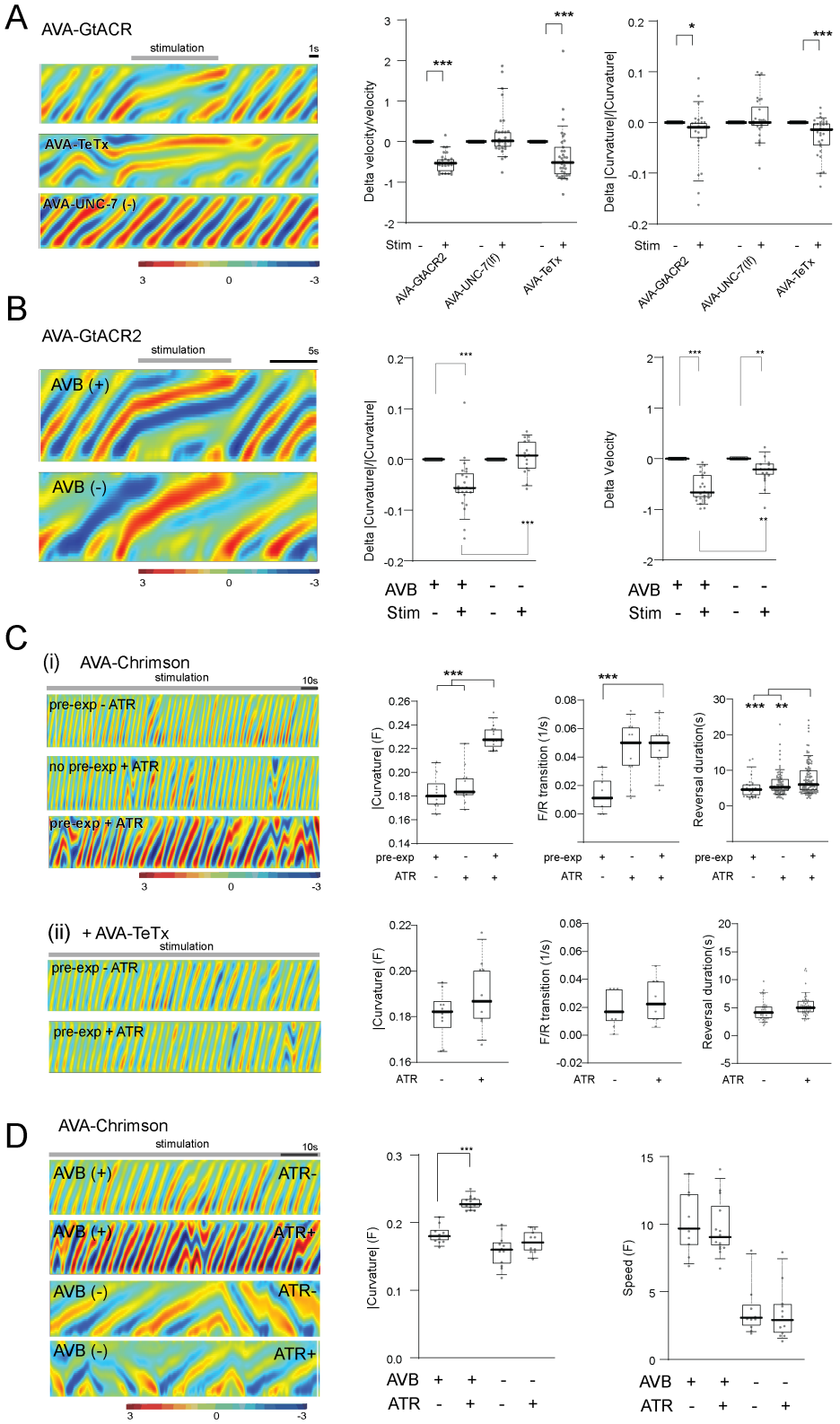

Figure 6. Tonic optogenetic stimulation of AVA potentiates forward locomotion in an AVB dependent manner.
A. (Left panel) representative heatmaps of curvature of AVA-specific GtACR2 animals (+ATR) in wildtype (Top panel), AVA-specific TeTx (mid panel) and AVA-specific UNC-7(lf); A-TWK-18(gf) (bottom panel) background animals. (Right panel) velocity and curvature changes upon light stimulation in each genotype. Upon AVA-specific GtACR2 weak stimulation, animals reduce velocity and curvature in wildtype and AVA-specific TeTx background. Loss of UNC-7 in AVA abolished such inhibition on the locomotion. **B.** (Mid and right panel) representative heatmaps of body curvature of control (LED non treated) and AVB ablated (LED retreated) animals of AVA-Specific GtACR2 background upon weak stimulation. (Mid and right panel) velocity changes and curvature changes in each genotype. Ablation of AVB partially abolished the effect of AVA-specific GtACR2 on the forward curvature and velocity. **C.** (i, left panel) representative heatmaps of curvature of AVA-specific Chrimson animals with green light pre-exposure but without ATR treatment (top panel, control), with ATR treatment but without green light pre-exposure (middle panel, weak activation), and with ATR treatment and green light pre-exposure (bottom panel, weak and tonic activation). (Right panel) averaged forward bending curvature, forward to backward transition frequency and reversal duration in each animals. Animals with weak stimulation (ATR treatment, weak light stimulation but without pre-exposure) only exhibit increased forward to reversal transitions. Animals with weak and tonic stimulation (ATR treatment, pre-exposure and weak light stimulation) exhibits increased forward to reversal transitions and increased curvature during forward movement. (ii), (Left panel) representative heatmaps of curvature of AVA-specific Chrimson; specific TeTx background animals with or without ATR treatment upon weak and tonic stimulation. (Right panel) averaged forward bending curvature, forward to backward transition frequency and reversal duration of AVA-specific Chrimson; specific TeTx animals. No significant changes were observed in all parameters. **D.**(Left panel) representative heatmaps of body curvature of control(wildtype background) and AVB ablated (LED treated) animals of AVA-Specific Chrimson background with and without ATR upon weak and tonic stimulation. (Mid and right panel) averaged forward curvature speed in each genotype. Ablation of AVB abolished the tonic effect of AVA-Chrimson on the forward curvature.

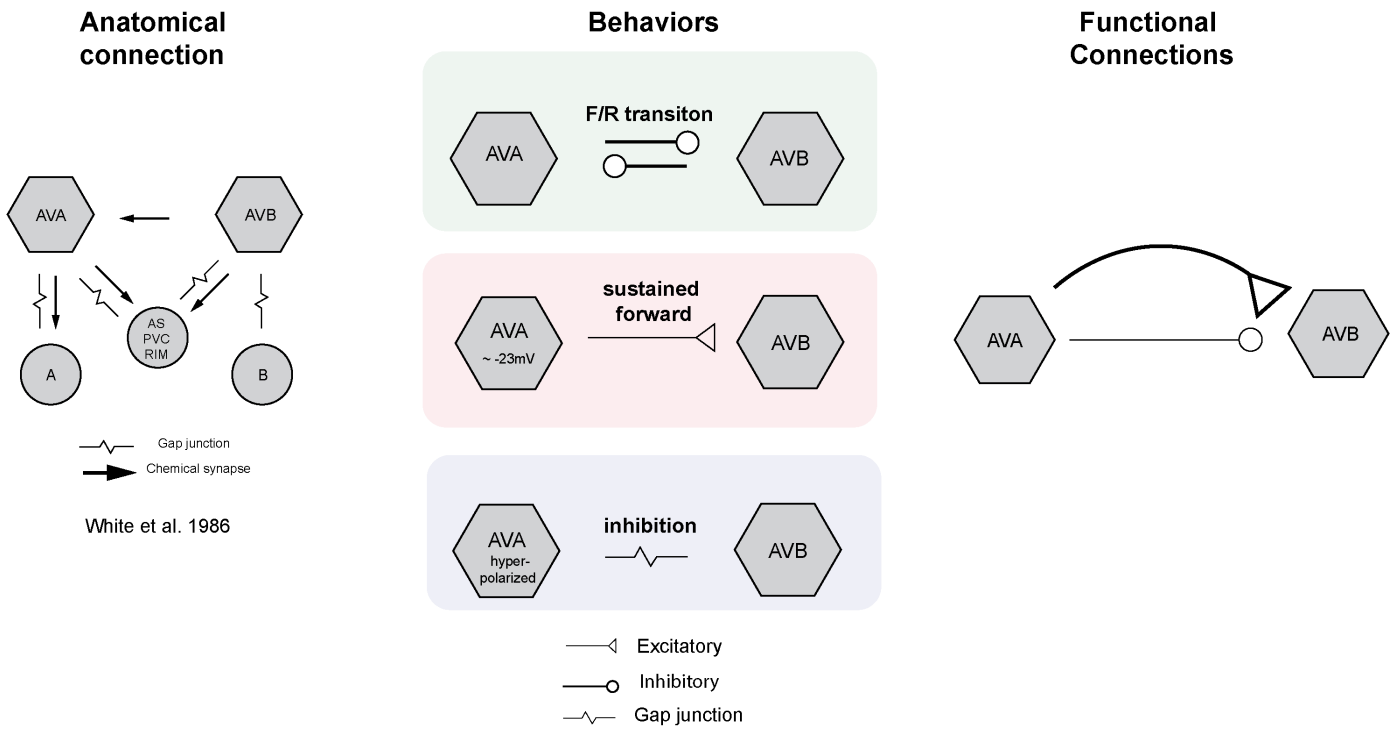

Figure 7. Anatomical and functional motifs of forward and backward movement in *C. elegans*.
(Left panel) Schematic of the anatomic wiring diagram between premotor interneurons and motor neurons implicated for forward (AVB, B, AS) and backward (AVA, A, AS) movement. (Mid panel) Schematic of the functional motifs of directional movement. During the forward/backward motor transition, AVA and AVB are likely reciprocal inhibited, the mechanisms of which are currently unknown. During forward movement, AVA maintains an unusually depolarized RMP which promotes AVB activity and forward movement. On the other hand, hyperpolarized AVA inhibits forward movement and AVB activity. (Right panel) our proposed model where AVA regulates backward and forward locomotion through phasic inhibition and tonic excitation of AVB respectively.

Supplemental figures

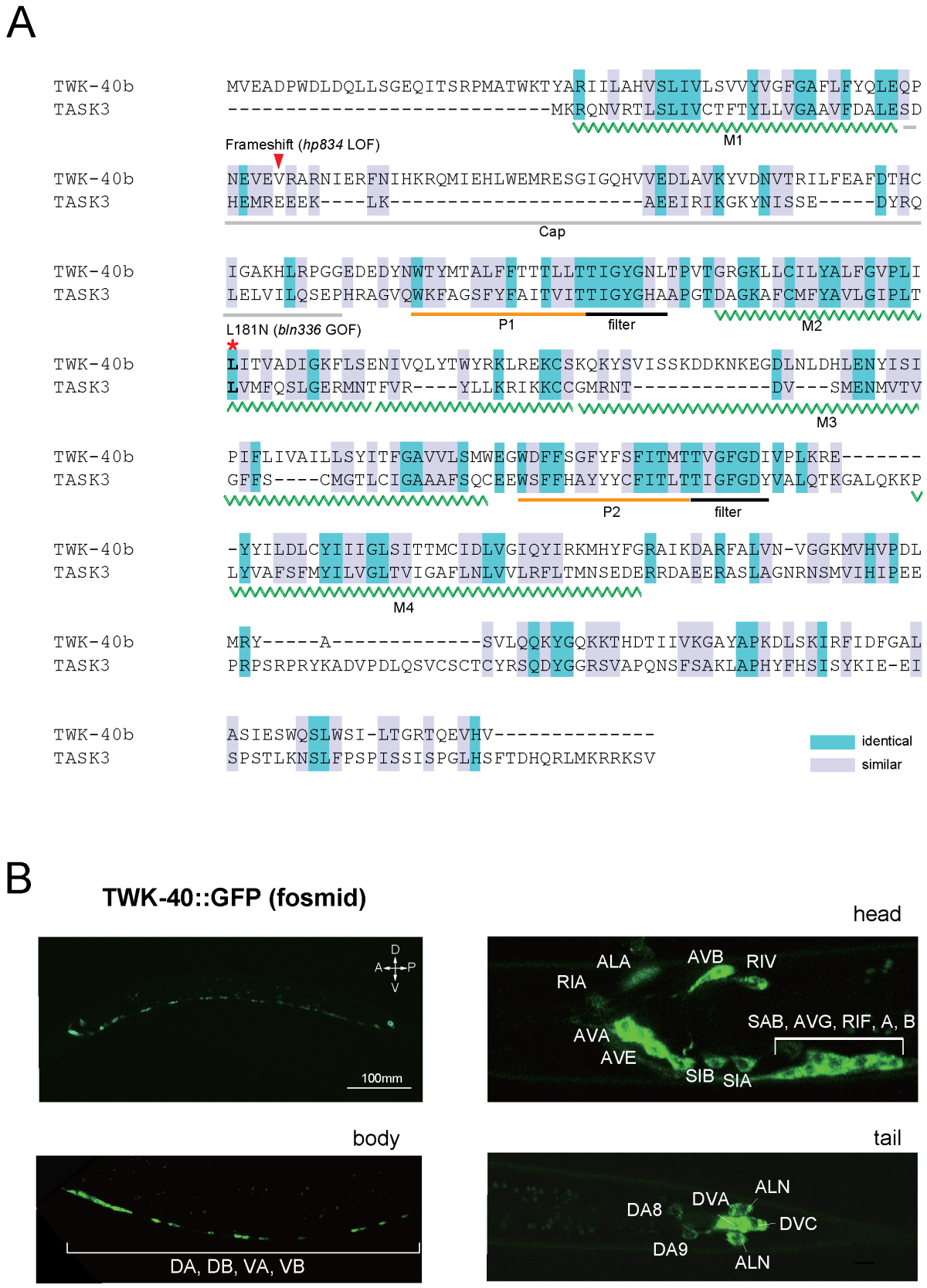

Figure 1S–1. Amino acid sequence alignment between and expression of TWK-40 fosmid.
A. Amino acid sequence alignment between TWK-40 and human TASK3. The predicted pore-forming P1 and P2 domains are denoted by the orange lines. Potassium selective filters are denoted by the black lines that are conserved among K2P channels. The cap domain is donated by the gray line. The transmembrane domains are denotes by the green zigzag lines. Mutations in gain-of-function allele *bln336*are denoted by *. A red arrowhead labels mutation in the null allele *hp834*; *hp834* is a 7bp exonal deletion that leads to a frameshift and a premature stop codon. The residues related to channel function are bolded and highlighted. **B.** Confocal images of a functional TWK-40 GFP fosmid reporter. It is expressed in 18 neuronal classes with a range of expression intensities. GFP in AVA is the strongest.

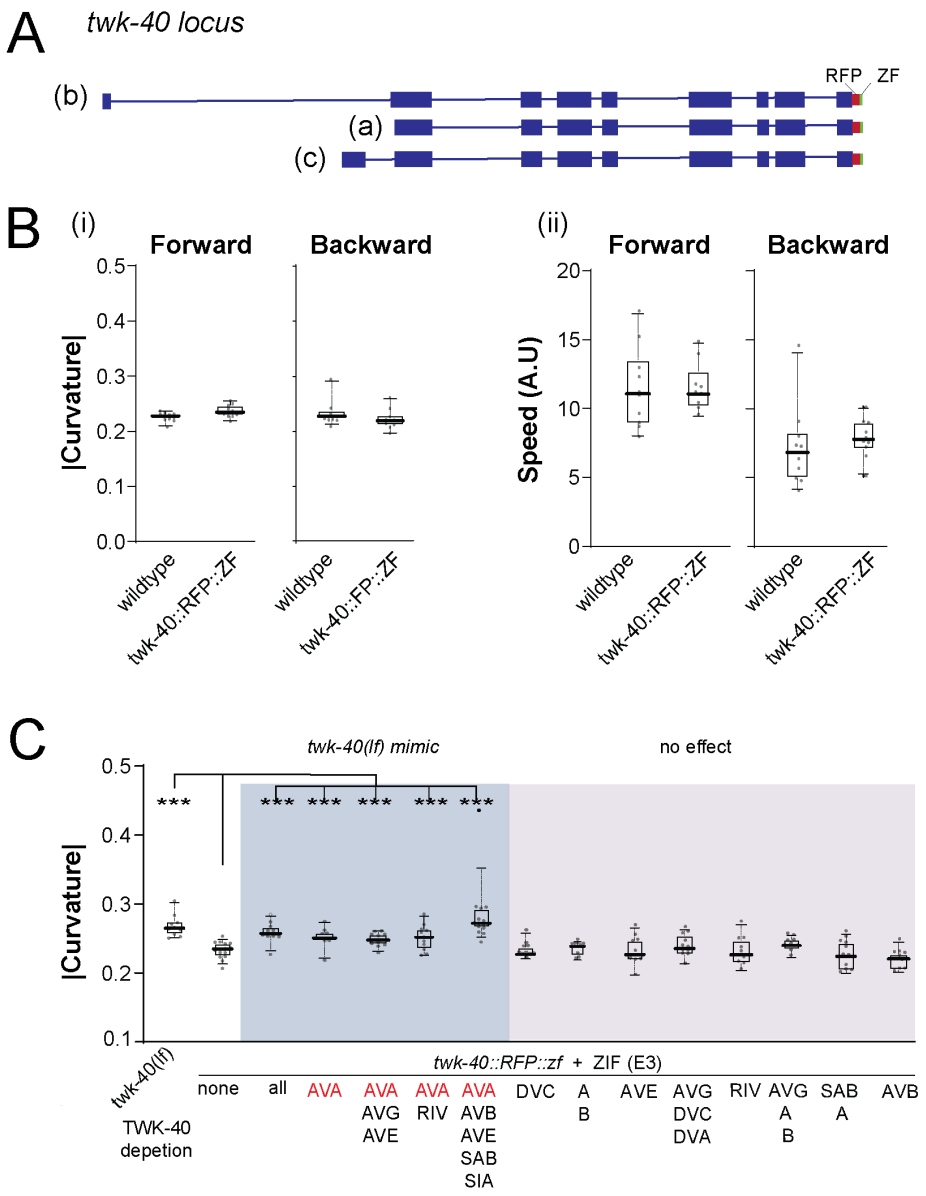

Figure 1S–2. TWK-40 mainly functions through AVA to regulate curvature during forward movement.
A. Gene structure of *twk-40* (isoform a, b and c). Blue boxes denote exons. Lines denote introns. Red and green boxes denote the insertion of tagRFP and ZF domain at the C-terminal of endogenous TWK-40. **B.** Averaged curvature (i) and speed (ii) in wildtype and *bln282 (twk-40::RFP::ZF)* animals. No significant differences were observed in *bln282* animals. **C.** Averaged curvature during forward movement in *twk-40(hp834; lf)*, *bln282* and animals upon cell-specific depletion of TWK-40. Only when ZIF-1 is expressed in AVA, animals exhibit increased forward bending.

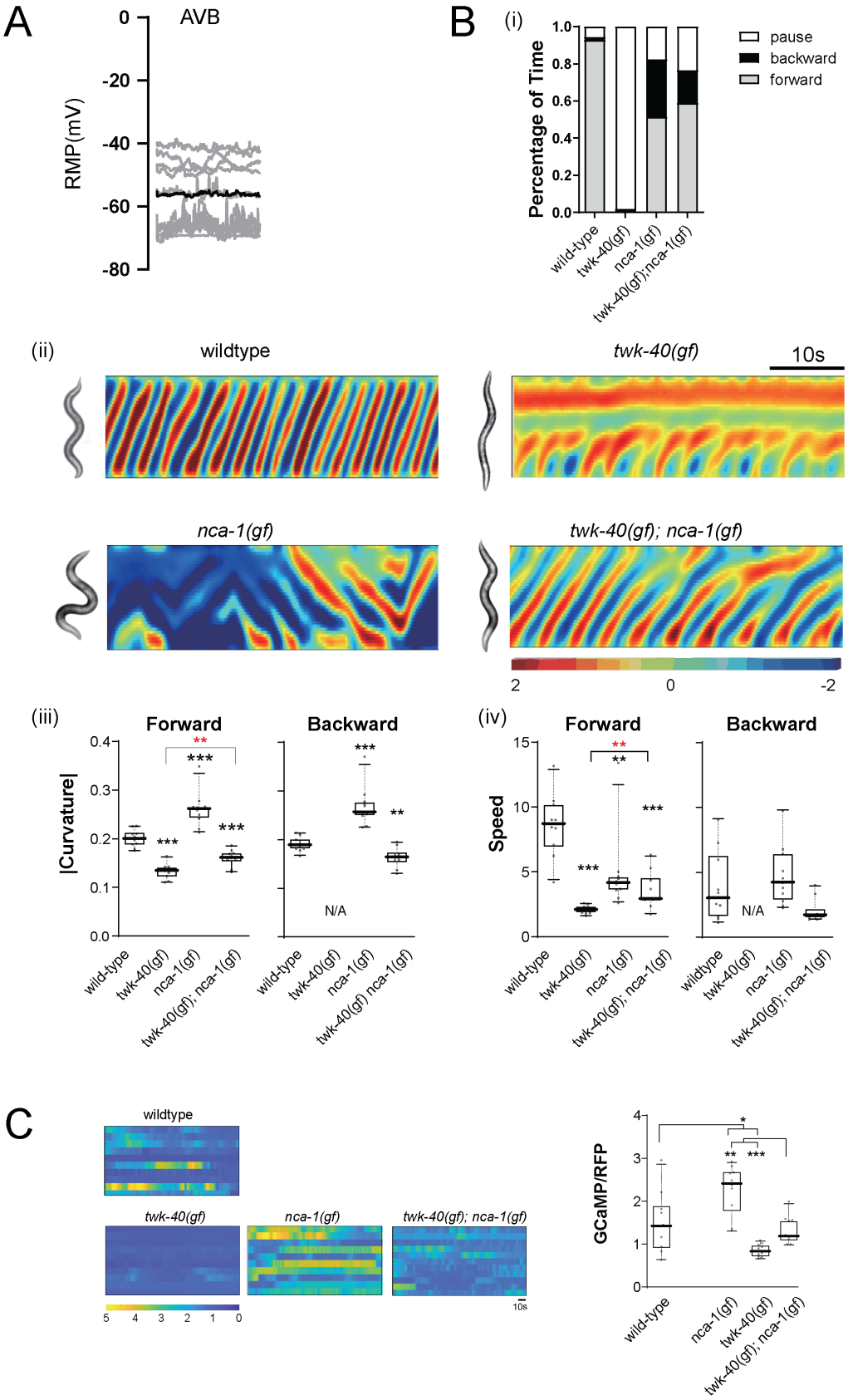

Figure S2. The TWK-40 K2P antagonizes the NCA sodium leak channel.

A. All along the averaged traces of AVB's RMP by whole-cell patch-clamp recordings in wildtype animals. AVB holds an averaged RMP -55mV, much more hyperpolarized than AVA. **B.** (i) movement propensity in each genotype. *nca-1(gf)* exhibit increased propensity of backward movement. (ii) representative heat map of curvature of freely moving animals of each genotype. (iii, iv) averaged curvature and speed during forward and backward movement in each genotype. *nca-1(gf)* partially suppresses the decreased curvature and speed during forward and back movement in *twk-40(gf)*. The comparison was against wildtype animals unless specified. **C.** (Left panel) raster plots of AVA soma activity in crawling animals of each genotype. *nca-1(gf)* exhibits increased calcium activity, partially restoring the activity level in *twk-40(gf); nca-q(gf)*. Each trace represents one animal. (Right panel) quantification of AVA's activity during all motor states in each genotype.

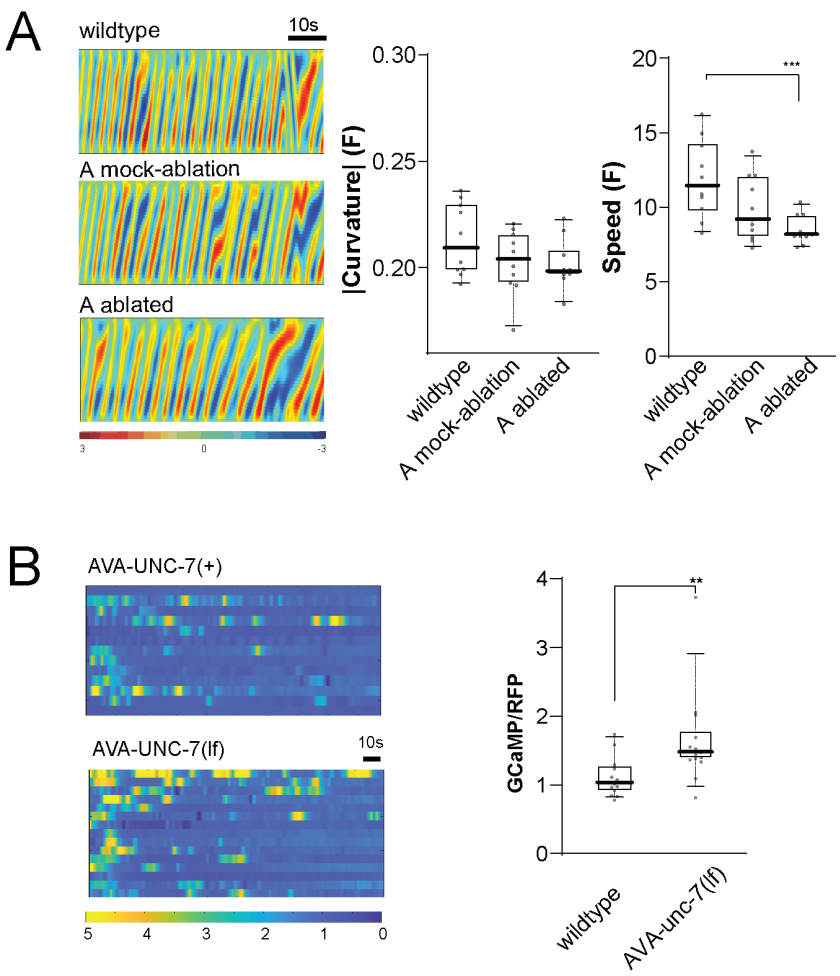

Figure S3. AVA maintains forward locomotory activity.

A. (Left panel) representative heatmaps of curvature, (mid panel) averaged forward curvature in wildtype, control (LED non treated), and A motor neuron ablated animals (*Punc-4-mito::miniSOG*, LED treated). There is no significant difference between the groups. (Mid and right panel) averaged curvature and speed during forward locomotion in wildtype, control (non LED treated), and A motor neuron ablated (LED treated) animals. There is no significant change in forward curvature. Forward speed is mildly but significantly decreased in A motor neuron ablated animals versus wildtype animals, but not significantly changed versus control animals. **B.** (Left panel) raster plot and (right panel) averaged AVA activity during all motor states , represented by the GCaMP/RFP ratio in free moving control (non Auxin treated; *unc-7*::AID; AVA-TIR1) and AVA-specific UNC-7(lf) (Auxin treated, *unc-7*::AID; AVA-TIR1) animals. AVA exhibits increased activities when UNC-7 is lost specifically from AVA. Each trace represents one animal.

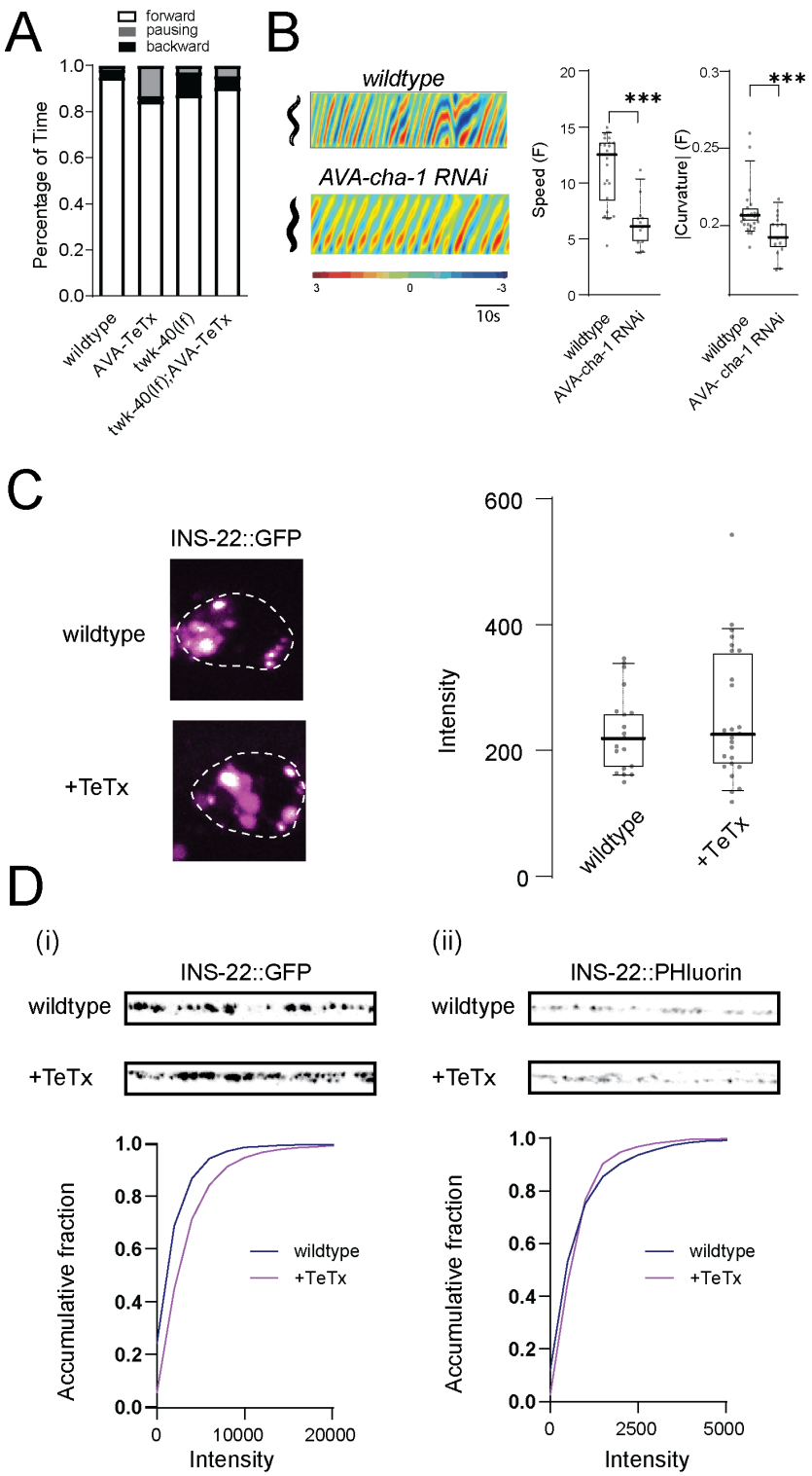

Figure S4. TeTx preferentially blocks neurotransmission.

A. Propensity of animals of each genotype in forward, backward and pausing states. **B.** Representative heatmaps of curvature (left panel), averaged forward speed (mid panel), and averaged forward curvature (right panel) of wildtype and AVA-specific *cha-1* RNAi animals. AVA- specific *cha-1* RNAi reduces animals' curvature and speed during forward movement. **C.** Maximum projection of confocal images of coelomocytes where secreted neuropeptides accumulate (*Pnpr-4-ins-22::GFP*) in wildtype and *Pnpr-4-TeTx* animals. Mean intensity of GFP in coelomocytes shows no differences in wildtype and *Pnpr-4-TeTx* animals. **D.** (i. top panel) maximum projection of a neuropeptide marker (INS-22::GFP) in AVA ventral cord. (i, lower panel) cumulative frequency of INS-22::GFP intensity, showing no significant changes in AVA-specific TeTx animals. (ii, top panel) maximum projection of a neuropeptide secretion marker (INS-22::PHluorin) in AVA in ventral cord showing no changes in AVA-specific TeTx. (ii, lower panel) Cumulative frequency of PHluorin intensity, showing no significant changes in AVA-specific TeTx.

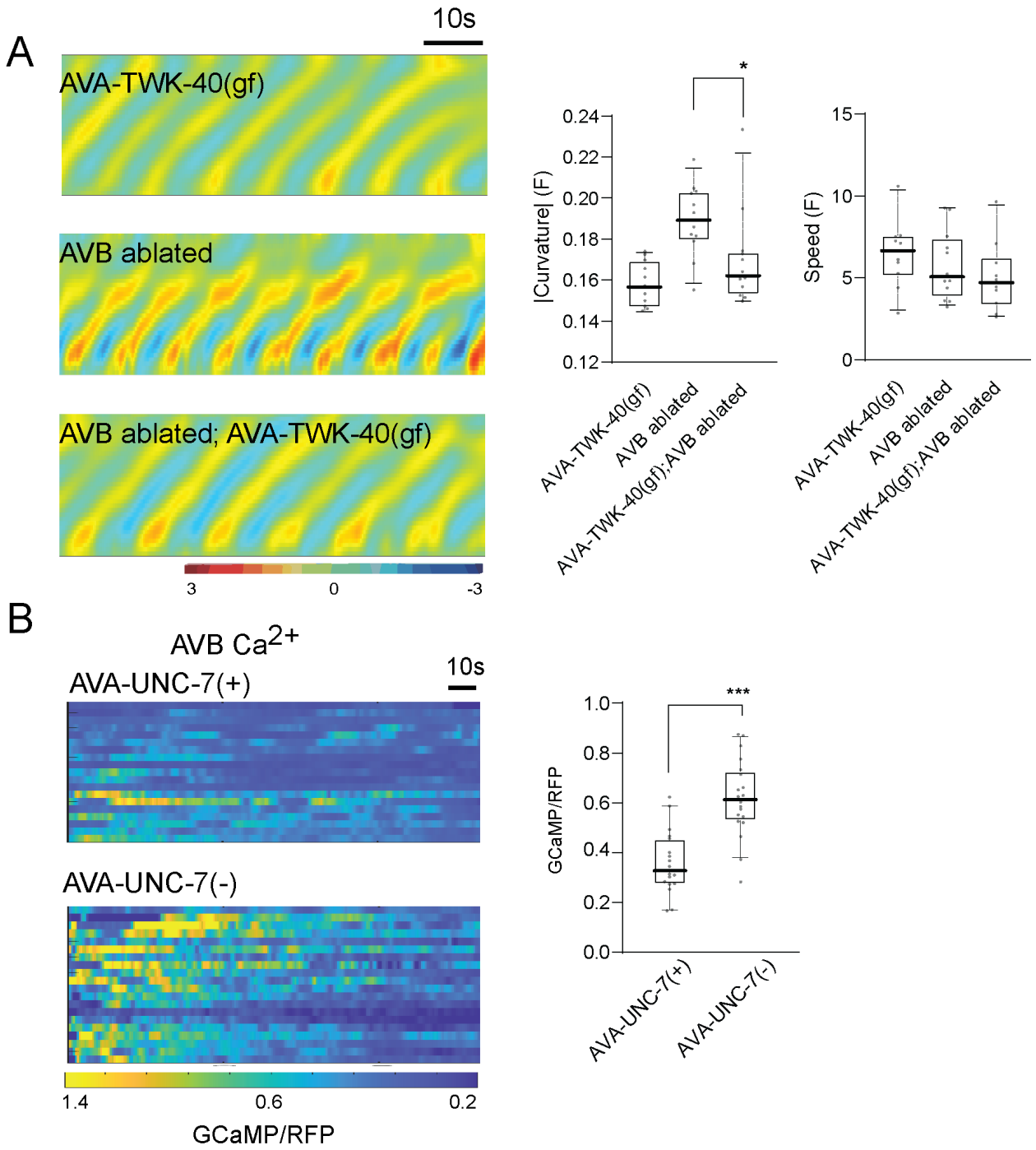

Figure S5. AVB ablation does not enhance the phenotype in AVA-Specific TWK-40(gf) animals. UNC-7 coupling dampens AVB's activity
A. (Left panel) representative heatmaps of body curvature of control(LED non treated) and AVB ablated (LED treated) animals of AVA-specific TWK-40(gf) background. Averaged curvature (mid panel) and speed (right panel) during forward movement in each genotype. AVB ablated animals in AVA-specific TWK-40(gf) background are similar to AVA-TWK-40(gf) animals. **B.** (Left panel) raster plot and (right panel) quantification of AVB activity during all motor states, represented by the GCaMP/RFP ratio in freely moving wildtype and AVA-specific UNC-7(lf) animals . Each trace represents one animal. AVB exhibits increased activities when UNC-7 is depleted specifically from AVA.

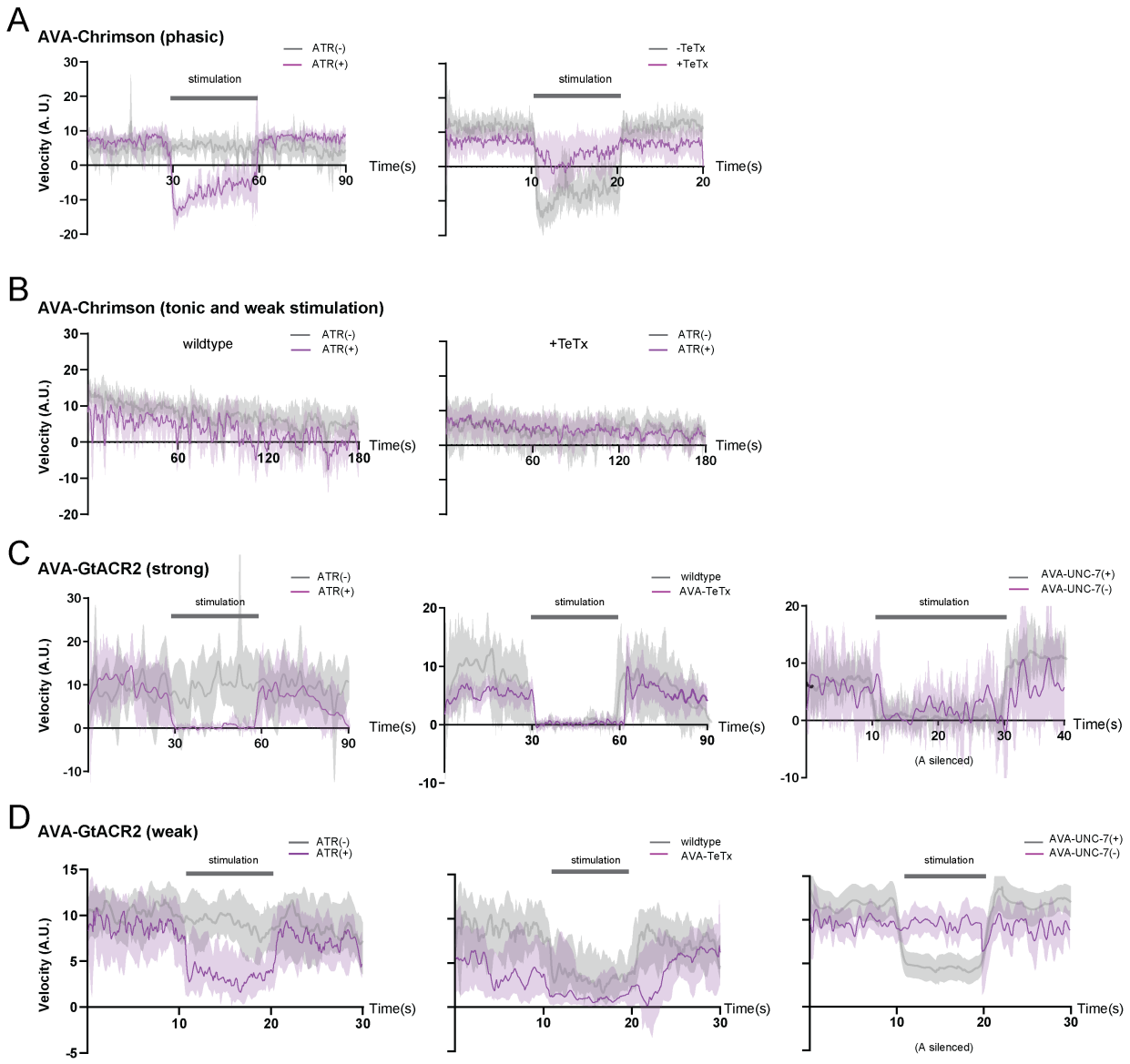

Figure S6. Velocity upon optogenetic manipulation of AVA.

A. B Traces of freely moving AVA-Chrimson animals upon phasic (A) and tonic/weak (B) stimulation in wild-type (left panel) and AVA-specific TeTx (right panel) background animals. The stimulation periods were denoted by the gray bar. Upon phasic stimulation, AVA-Chrimson animals exhibit sustained reversals. AVA-Specific TeTx attenuate the sustained reversal. **C. D.** Traces of freely moving AVA-Specific GtACR2 animals upon strong (A) and weak (B) stimulation in wildtype (left panel), AVA-specific TeTx (mid panel), and AVA-specific UNC-7(lf); A-TWK-18(gf) (right panel) background animals. Stimulation periods were denoted by the gray bar. Upon strong stimulation, AVA-specific GtACR2 animals halt. Such halt can not be completely blocked by AVA-Specific TeTx or AVA-Specific UNC-7(lf). While, upon weak stimulation, AVA-specific GtACR2 animals reduce velocity. Such halt can not be partially blocked by AVA-Specific TeTx and completely blocked by AVA-Specific UNC-7(lf).